

AD-A084 347

MISSISSIPPI UNIV UNIVERSITY

F/6 20/14

ELECTROMAGNETIC SCATTERING BY SURFACE OF ARBITRARY SHAPE.(U)

MAR 80 D R WILTON; S S RAO; A W GLISSON

F30602-78-C-0148

UNCLASSIFIED

RADC -TR-79-325

NL

AD-A084 347

END
DATE
FILMED
6-80
DTIC

LEVEL #



RADC-TR-79-325

Phase Report

March 1980



ADA 084347

ELECTROMAGNETIC SCATTERING BY SURFACES OF ARBITRARY SHAPE

University of Mississippi

**Donald R. Wilton
S. S. M. Rao
Allen W. Glisson**

APPROVED FOR PUBLIC RELEASE; DISTRIBUTION UNLIMITED

**DTIC
ELECTE
S MAY 20 1980 D
A**

**ROME AIR DEVELOPMENT CENTER
Air Force Systems Command
Griffiss Air Force Base, New York 13441**

FILE COPY

80 5 19 017

This report has been reviewed by the RADC Public Affairs Office (PAO) and is releasable to the National Technical Information Service (NTIS). At NTIS it will be releasable to the general public, including foreign nations.

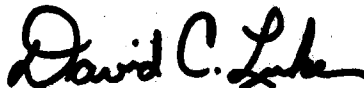
RADC-TR-79-325 has been reviewed and is approved for publication.

APPROVED:



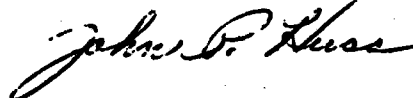
JOHN H. EDWARDS, JR.
Project Engineer

APPROVED:



DAVID C. LUKE, Lt Col, USAF
Chief, Reliability & Compatibility Division

FOR THE COMMANDER:



JOHN P. HUSS
Acting Chief, Plans Office

If your address has changed or if you wish to be removed from the RADC mailing list, or if the addressee is no longer employed by your organization, please notify (RBCA), Griffiss AFB NY 13441. This will assist us in maintaining a current mailing list.

Do not return this copy. Retain or destroy.

UNCLASSIFIED

SECURITY CLASSIFICATION OF THIS PAGE (When Data Entered)

REPORT DOCUMENTATION PAGE		READ INSTRUCTIONS BEFORE COMPLETING FORM	
1. REPORT NUMBER RADC-TR-79-325	2. GOVT ACCESSION NO. AD-A084347	3. RECIPIENT'S CATALOG NUMBER	
4. TITLE (and Subtitle) ELECTROMAGNETIC SCATTERING BY SURFACE OF ARBITRARY SHAPE	5. TYPE OF REPORT & PERIOD COVERED Phase Report	6. PERFORMING ORG. REPORT NUMBER N/A	
7. AUTHOR(S) Donald R. Wilton S. S. M. Rao Allen W. Glisson	8. CONTRACT OR GRANT NUMBER(s) F30602-78-C-0148	9. PROGRAM ELEMENT, PROJECT, TASK AREA & WORK UNIT NUMBERS 62702F 233803	
10. PERFORMING ORGANIZATION NAME AND ADDRESS University of Mississippi University MS 38677	11. CONTROLLING OFFICE NAME AND ADDRESS Rome Air Development Center (RBCA) Griffiss AFB NY 13441	12. REPORT DATE March 1980	
13. MONITORING AGENCY NAME & ADDRESS (if different from Controlling Office) Same	14. SECURITY CLASS. (of this report) UNCLASSIFIED	15. DECLASSIFICATION DOWNGRADING SCHEDULE N/A	
16. DISTRIBUTION STATEMENT (of this Report) Approved for public release; distribution unlimited.			
17. DISTRIBUTION STATEMENT (of the abstract entered in Block 20, if different from Report) Same			
18. SUPPLEMENTARY NOTES RADC Project Engineer: John H. Edwards, Jr. (RBCA) This work was performed while the first two authors were at Syracuse University, Syracuse, New York, during the 1978-1979 academic year.			
19. KEY WORDS (Continue on reverse side if necessary and identify by block number) Electromagnetic Compatibility Electromagnetics EM Scattering Numerical Analysis EM Field Equations			
20. ABSTRACT (Continue on reverse side if necessary and identify by block number) In this report the electric field integral equation (EFIE) is used with the moment method to develop a simple and efficient numerical procedure for treating problems of scattering by arbitrarily-shaped objects. The objects are modeled for numerical purposes by planar triangular surface patch models. Because the EFIE formulation is used, the procedure is applicable to both open and closed bodies. Crucial to the formulation is the development of a set of special subdomain basis functions defined			

DD FORM 1 JAN 73 1473 EDITION OF 1 NOV 65 IS OBSOLETE

UNCLASSIFIED

(Cont'd)

SECURITY CLASSIFICATION OF THIS PAGE (When Data Entered)

234450

Shu

UNCLASSIFIED

SECURITY CLASSIFICATION OF THIS PAGE(When Data Entered)

Item 20 (Cont'd)

on pairs of adjacent triangular patches. The basis functions yield a current representation which is free of line or point charges at sub-domain boundaries.

A second approach using the magnetic field integral equation (MFIE) and employing the same basis functions is also developed. Although the MFIE applies only to closed bodies, the moment matrix of the MFIE is also needed in dielectric scattering problems and in the so-called combined field integral equation used to eliminate difficulties with internal resonances present in the MFIE and EFIE formulations.

The EFIE approach is applied to the scattering problems of plane wave illumination of a flat square plate, a bent square plate, a circular disk, and a sphere. Comparisons of surface current densities are made with previous computations or exact formulations and good agreement is obtained in each case. The MFIE approach is also applied to the sphere and reasonable agreement with exact calculations is obtained.

A

UNCLASSIFIED

SECURITY CLASSIFICATION OF THIS PAGE(When Data Entered)

TABLE OF CONTENTS

1. INTRODUCTION	1
2. ELECTRIC FIELD FORMULATION	6
Electric Field Integral Equation	6
Development of Basis Functions	7
Testing Procedure	14
Evaluation of Matrix Elements	17
3. MAGNETIC FIELD FORMULATION	24
Magnetic Field Integral Equation	24
Expansion and Testing Procedure	25
Evaluation of Matrix Elements	26
4. NUMERICAL RESULTS	28
Flat Plate	28
Bent Plate	32
Circular Disk	32
Sphere	32
5. SUMMARY	39
APPENDIX A. TOPOLOGICAL PROPERTIES AND MATHEMATICAL REPRESENTATION OF TRIANGULATED SURFACES	40
APPENDIX B. EVALUATION OF INTEGRALS APPEARING IN THE ELECTRIC FIELD FORMULATION	50
REFERENCES	61

Accession For	
NTIS Grant	<input checked="" type="checkbox"/>
DDC PAT	<input type="checkbox"/>
Unpublished	<input type="checkbox"/>
Journal Article	<input type="checkbox"/>
Other	<input type="checkbox"/>
<div style="text-align: center; font-size: 2em; font-family: cursive;">A</div>	

LIST OF FIGURES

Figure #	Caption	Page
1.	Arbitrary surface modeled by triangular patches.	4
2.	Local coordinates associated with an edge.	8
3.	Geometry showing normal component of basis function at edge.	11
4.	Geometry of vectors to centroids of triangles associated with an edge.	13
5.	Edges and local coordinates associated with a triangle.	15
6.	Local coordinates and edges for source triangle T^q with observation point in triangle T^p .	20
7.	Definitions of areas used in defining area coordinates.	22
8.	Distribution of dominant component of current on 0.15λ square flat plate.	29
9.	Distribution of dominant component of current on a 1.0λ square flat plate.	30
10.	Distribution of dominant component of current on a 0.15λ bent square plate.	33
11.	Distribution of dominant component of current on a 1.0λ bent square plate.	34
12.	Distribution of current on a 0.05λ radius circular disk.	35
13.	Distribution of current components on a 0.2λ radius conducting sphere calculated by an electric field integral equation formulation.	36
14.	Distribution of current components on a 0.2λ radius conducting sphere calculated by a magnetic field integral equation formulation.	37
A1.	Arbitrary surface modeled by triangular patches.	42
A2.	Auxiliary vertices and edges used to close apertures to form a closed body.	44
A3.	Relationship between face and edge orientations and current reference direction at an edge.	49

I. INTRODUCTION

Since the very beginning of the application of numerical methods to electromagnetics, there has been a keen interest in developing computer codes for treating radiation and scattering problems involving arbitrarily-shaped conducting bodies. Of the various possible approaches available to developers of such codes, the most commonly used have been wire-grid and surface patch modeling in conjunction with integral equation formulations.

The wire-grid modeling approach has been remarkably successful in many problems, particularly in those requiring the prediction of far-field quantities such as radiation patterns and radar cross-sections [1]. The approach is not as well-suited for calculating near-field and surface quantities, such as surface current and input impedance, however. Some of the difficulties encountered in wire-grid modeling include the occasional presence of fictitious loop currents in the solution, difficulties with internal resonances [2], and problems of relating computed wire currents to equivalent surface currents. The accuracy of wire-grid modeling has also been questioned on theoretical grounds [3]. These difficulties have provided strong incentives for developing surface patch approaches as alternatives to wire-grid techniques.

Several approaches to surface patch modeling have been suggested. Knepp and Goldhirsh [4] partition a surface into non-planar quadrilateral patches and employ the magnetic field integral equation (MFIE) to solve the electromagnetic problem. Albertsen et al. [5] solve for the current and compute radiation patterns for satellite structures with attached wire antennas, booms, and solar panels. They use the MFIE with planar quadrilateral surface patches to model the satellite, and use the electric field integral equation (EFIE)

to treat the wire antennas in their hybrid formulation. The arbitrary surface treatment of the widely-used Numerical Electromagnetic Code (NEC) developed at the Lawrence Livermore Laboratory [6] is also based on the formulation of Albersen et al. Wang et al. [7] extend the use of piecewise-sinusoidal basis functions, well-known in wire analyses, to the treatment of surfaces. They use an EFIE formulation and model surfaces by planar rectangular patches. Sankar and Tong [8] employ planar triangular patches to model a square plate and point out the possibility of extending their approach to arbitrary bodies. Their formulation, based on a variational formula for the current which is made stationary with respect to a set of trial functions, is equivalent to a Galerkin solution of the EFIE. Wang [9,10] employs planar triangular patches in conjunction with the MFIE and uses basis functions which contain the phase variation of the incident field in each patch. Unfortunately, this procedure makes the resultant moment matrix depend on the incident field. Jeng et al. [11] propose using the MFIE and non-planar triangles to model arbitrary surfaces. Singh and Adams [12] propose using planar quadrilateral patches and sinusoidal basis functions with the EFIE.

In arbitrary surface modeling, the EFIE has the advantage that it applies to both open and closed bodies, whereas the MFIE applies to closed bodies only. On the other hand, for arbitrarily-shaped objects the EFIE is much more difficult to deal with, as attested to by the fact that of the EFIE formulations discussed, only Wang et al. have actually treated non-planar structures--and their formulation is limited to structures with curvature in one dimension only. The difficulties with the EFIE stem primarily from the presence of derivatives and a singular kernel in the integral equation. One manifestation of the derivatives is that if basis functions representing the current are not

constructed such that their normal components are continuous across surface edges, then line or point charges are deposited along the edges. If present, these fictitious charges usually lead to deleterious effects in the solution. The approach of Wang et al. [7] is, as they point out, free of these difficulties, but their use of rectangular patches restricts their consideration to (finite) cylindrical surfaces. More appropriate for modeling arbitrarily-shaped surfaces are planar triangular patch models such as shown in Fig. 1.

Some of the advantages of triangular patch surface modeling have been noted by Sankar and Tong [8], as well as Wang [9]. For example, triangular patches have the ability to conform to any geometrical surface and boundary, they permit simple descriptions of the surface and patch scheme to the computer, and they may be used with greater patch densities on those portions of the surface where more resolution is desired. (Although planar quadrilateral patch modeling shares many of these features, the vertices of planar quadrilaterals may not be independently specified because all four vertices must lie in the same plane.)

In this report we use planar triangular patch modeling and apply the method of moments [13] to develop numerical procedures for both the EFIE and MFIE formulations. The computer code based on the EFIE is capable of handling either open or closed and arbitrarily-curved structures of finite extent. Discounting limitations of the computer, the code can, in fact, treat any object whose surface is orientable, connected (i.e., the body does not comprise, in reality, two or more separate objects), and free of intersecting surfaces. Not only open and closed surfaces, but also multiply-connected objects such as the structure with a "handle" (c.f. Appendix A) shown in Fig. 1 are admissible. The computer code based on the MFIE has the same range of

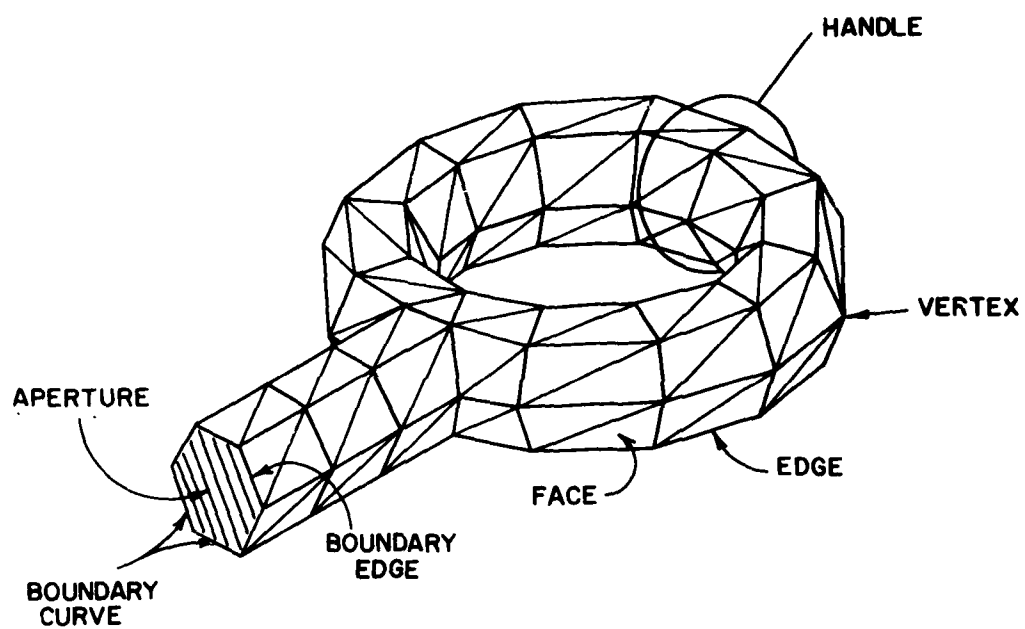


Fig. 1. Arbitrary surface modeled by triangular patches.

applicability, except that it is restricted to closed surfaces. Both the EFIE and MFIE approaches developed are simple and efficient to apply.

We remark that a previous paper has considered the electrostatic problem of determining the charge distribution on arbitrarily-shaped conducting bodies modeled by triangular patches [14]. We note also that the formulation used there is related to the static limit of the present EFIE formulation and that both formulations employ piecewise constant charge representations.

In the following section, we present the EFIE formulation. A new set of basis functions defined on triangular patches is described and used to represent the current in the moment method. These new basis functions are free of fictitious line or point charges and are analogous to the so-called "rooftop" functions defined on planar rectangular subdomains [15].

The MFIE formulation, which also makes use of these new basis functions, is presented in Section III. Despite its lack of generality, the MFIE formulation is important because its moment matrix is required in problems of scattering by dielectric objects [16], and in the so-called combined field integral equation formulation [17]. The latter is a technique for eliminating difficulties in both the EFIE and MFIE formulations for scattering problems at frequencies corresponding to the cavity resonances of the interior region for closed surfaces.

In Section IV, numerical results obtained using the EFIE formulation are presented for triangular patch models of a flat square plate, a bent rectangular plate, a circular disk, and a sphere. Results obtained using the MFIE are also presented for the sphere problem.

II. ELECTRIC FIELD FORMULATION

In this section, we derive an integral equation for the surface current induced on a conducting scatterer from the boundary conditions on the electric field. A set of expansion functions and a testing procedure are then developed for use in applying the method of moments, and the moment matrix is derived. Finally, the evaluation of elements of the moment matrix is discussed.

Electric Field Integral Equation

Let S denote the surface of an open or closed, perfectly conducting scatterer. An electric field \vec{E}^i , defined in the absence of the scatterer, is incident and induces surface currents \vec{J} on S . If S is open, we regard \vec{J} at each point as the vector sum of the currents on opposite sides of the surface. We can compute the scattered electric field \vec{E}^s from the surface current by

$$\vec{E}^s = -j\omega\vec{A} - \nabla\phi \quad (1)$$

where the magnetic vector potential is defined as

$$\vec{A}(\vec{r}) = \frac{\mu}{4\pi} \int_S \vec{J} \frac{e^{-jkR}}{R} dS' \quad (2)$$

and the scalar potential is

$$\phi(\vec{r}) = \frac{1}{4\pi\epsilon} \int_S \sigma \frac{e^{-jkR}}{R} dS'. \quad (3)$$

An $\exp(j\omega t)$ time dependence is assumed and suppressed, and $k = \omega\sqrt{\mu\epsilon} = 2\pi/\lambda$, where λ is the wavelength. The permeability and permittivity of the surrounding medium are μ and ϵ , respectively, and $R = |\bar{r} - \bar{r}'|$ is the distance between an arbitrarily-located observation point \bar{r} and a source point \bar{r}' located on S . Both \bar{r} and \bar{r}' are defined with respect to a global coordinate origin O . The surface charge density σ is related to the surface divergence of \bar{J} through the equation of continuity,

$$\nabla_s \cdot \bar{J} = -j\omega\sigma. \quad (4)$$

We derive the integro-differential equation for \bar{J} by applying the boundary condition $\hat{n} \times (\bar{E}^i + \bar{E}^s) = \bar{0}$ on S , obtaining,

$$-\bar{E}_{\text{tan}}^i = (-j\omega\bar{A} - \nabla\Phi)_{\text{tan}}, \bar{r} \text{ on } S. \quad (5)$$

Eq. (5), with (2) - (4), constitutes the so-called electric field integral equation (EFIE). One notes that the presence of derivatives on the current in (4) and on the scalar potential in (5) suggests that one should be careful in selecting the expansion functions and testing procedure in the method of moments. In the next section, we choose expansion functions which yield a continuous current and a piecewise constant charge representation.

Development of Basis Functions

In this section, we discuss a set of basis functions, originally proposed by Glisson [18], which are suitable for use with the EFIE and triangular patch modeling. We assume a suitable triangulation approximating S and defined by a set of faces, edges, vertices, and boundary edges (c.f. Fig. 1).

Fig. 2 shows two triangles, T_n^+ and T_n^- , associated with the n^{th} edge of a

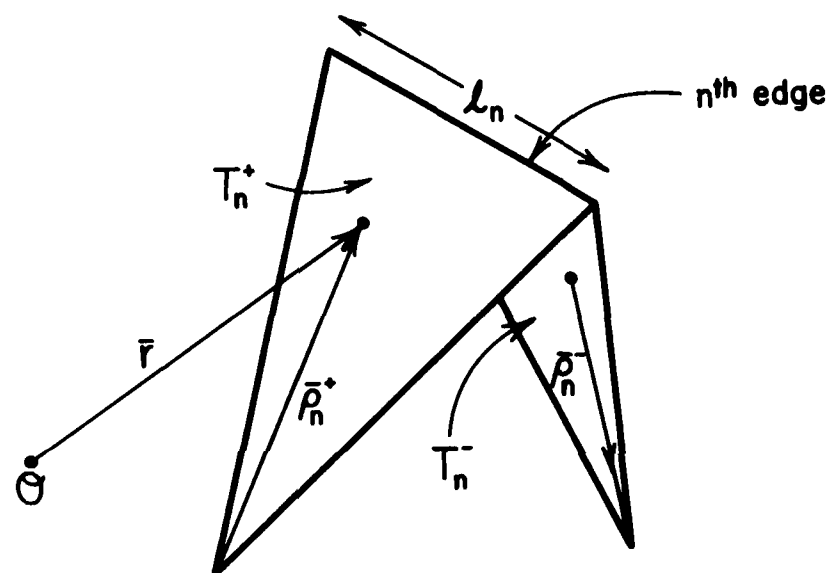


Fig. 2. Local coordinates associated with an edge.

triangulated surface modeling a scatterer. Points in T_n^+ may be designated either by the position vector \bar{r} , defined with respect to 0, or by the position vector $\bar{\rho}_n^+$, defined with respect to the free vertex of T_n^+ . Similar remarks apply to the position vector $\bar{\rho}_n^-$ except that it is directed toward the free vertex of T_n^- . It is assumed that the plus or minus designation of the triangles has been chosen such that the positive current reference direction (c.f. Appendix A) associated with the n^{th} edge is from T_n^+ to T_n^- . We define a vector basis function associated with the n^{th} edge as

$$\bar{f}_n(\bar{r}) = \begin{cases} \frac{\ell_n}{2A_n^+} \bar{\rho}_n^+ & , \bar{r} \text{ in } T_n^+ \\ \frac{\ell_n}{2A_n^-} \bar{\rho}_n^- & , \bar{r} \text{ in } T_n^- \\ 0 & , \text{ otherwise,} \end{cases} \quad (6)$$

where ℓ_n is the length of the edge and A_n^\pm is the area of triangle T_n^\pm . (Note that we use the convention, followed throughout the report, that subscripts refer to edges while superscripts refer to faces.) The new basis function \bar{f}_n is to be used to approximately represent the current, and we list here some of its properties which make it uniquely suited to this role:

- i) The current has no component normal to any of the edges except the common edge (edge n) of T_n^+ and T_n^- ; were this not the case, the continuity equation (4) would demand the presence of line charges along these edges.
- ii) The surface divergence of the basis current, which is proportional

to the surface charge density, is

$$\nabla_s \cdot \bar{f}_n = \begin{cases} \frac{\ell_n}{A_n^+} & , \bar{r} \text{ in } T_n^+ \\ -\frac{\ell_n}{A_n^-} & , \bar{r} \text{ in } T_n^- \\ 0 & , \text{otherwise,} \end{cases} \quad (7)$$

where the surface divergence in T_n^\pm is $(\pm 1/\rho_n^\pm) \partial(\rho_n^\pm f_n)/\partial \rho_n^\pm$. The charge density is thus constant in each triangle, the total charge associated with the triangle pair T_n^+ and T_n^- is zero, and the basis functions for the charge evidently have the form of a pulse doublet [15].

- iii) The component of current crossing the n^{th} edge is continuous, and hence no line charge exists there; this may be seen by Fig. 3 which shows that the normal component of $\bar{\rho}_n^\pm$ along edge n is just the height of triangle T_n^\pm with edge n as the base and with the height expressed as $(2A_n^\pm)/\ell_n$. These factors are used to normalize \bar{f}_n such that its flux density normal to edge n is unity in (6), hence ensuring continuity of current normal to the edge.

- iv) The moment of \bar{f}_n is given by $(A_n^+ + A_n^-) \bar{f}_n^{\text{avg}}$ where

$$\begin{aligned} (A_n^+ + A_n^-) \bar{f}_n^{\text{avg}} &= \int_{T_n^+ + T_n^-} \bar{f}_n dS = \frac{\ell_n}{2} (\bar{\rho}_n^{c+} + \bar{\rho}_n^{c-}) \\ &= \ell_n (\bar{r}_n^{c+} - \bar{r}_n^{c-}) \end{aligned} \quad (8)$$

and $\bar{\rho}_n^{c\pm}$ is defined between the free vertex and the centroid of T_n^\pm with $\bar{\rho}_n^{c+}$ directed away from the vertex and $\bar{\rho}_n^{c-}$ directed toward

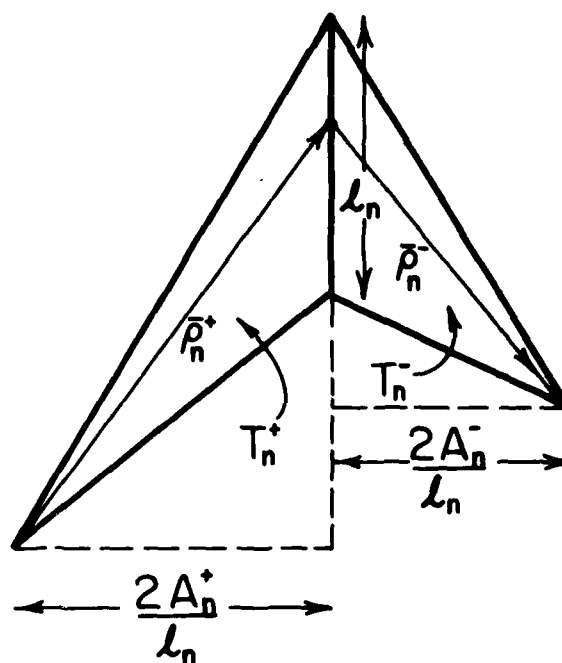


Fig. 3. Geometry showing normal component of basis function at edge.

the vertex, as shown in Fig. 4, and \bar{r}_n^{ct} is the vector from 0 to the centroid of T_n^+ ; Eq. (8) may be most easily verified by expressing the integral therein in terms of area coordinates, which are discussed later in this report.

Except for boundary edges, a basis function \bar{f}_n is associated with each edge of the triangulated structure. The current on S may be approximated in terms of the \bar{f}_n as

$$\bar{J} \approx \sum_{n=1}^N I_n \bar{f}_n(\bar{r}) \quad (9)$$

where N is the number of edges not on a surface boundary. Since a basis function is associated with each non-boundary edge, up to three non-zero basis functions may exist within each triangular face. At each edge, however, only the basis function associated with that edge may have a component of current normal to the edge; by (i), all other basis currents in that face are parallel to the edge. Furthermore, since the normal component of \bar{f}_n at the n^{th} edge is unity, each coefficient I_n in (9) may be interpreted as the normal component of current density flowing past the n^{th} edge. Because the normal component of current at a surface boundary must vanish anyway, we need not bother to define basis functions associated with boundary edges, and hence (9) includes only contributions from non-boundary edges.

The radial nature of the current flow associated with each basis function is at first disconcerting--certainly for a small triangle modeling a smooth section of the scatterer surface, one would not expect the direction of the actual current to vary substantially within the triangle. Turning the question around, one might ask, "Can a superposition of the basis functions within a triangle represent, say, a constant vector in the triangle?" That the

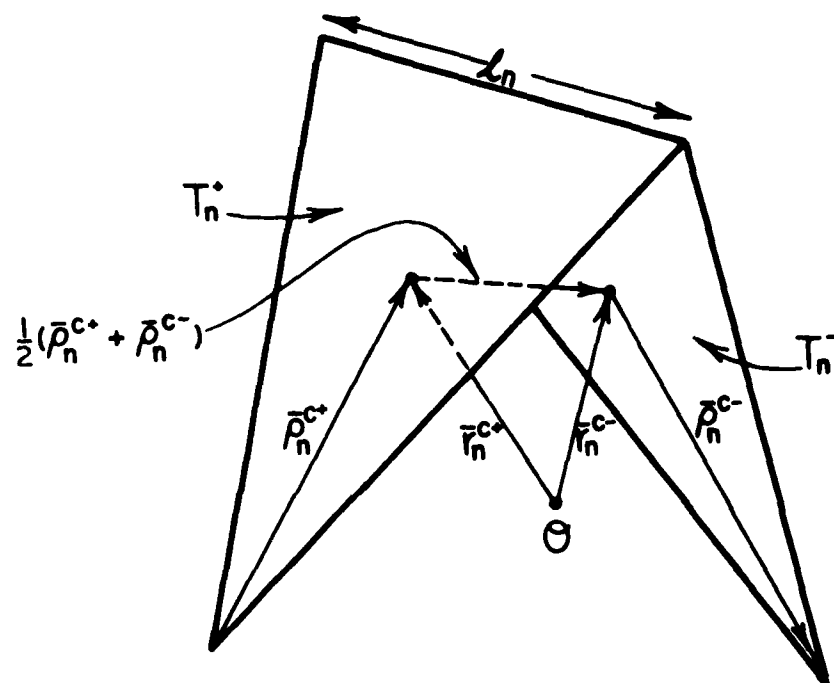


Fig. 4. Geometry of vectors to centroids of triangles associated with an edge.

answer is affirmative can be seen with the aid of Fig. 5, which shows a triangle T with the edges arbitrarily labeled 1, 2, and 3. With the vectors $\bar{\rho}_1$, $\bar{\rho}_2$, and $\bar{\rho}_3$ as shown, the basis functions in T are $\bar{f}_i = (\ell_i/2A) \bar{\rho}_i$, $i = 1, 2, 3$, where A is the triangle area and where, for simplicity, we assume that the current reference directions are out of the triangle for each edge. It is apparent from the definition of \bar{f}_i and the figure that the linear combinations $\ell_2 \bar{f}_1 - \ell_1 \bar{f}_2$ and $\ell_3 \bar{f}_1 - \ell_1 \bar{f}_3$ are constant vectors for every point \bar{r} inside the triangle and are parallel to sides 3 and 2, respectively. Since the two composite forms are linearly independent (i.e., non-parallel), a constant vector of arbitrary magnitude and direction within the triangle may be synthesized by an appropriate linear combination of the two forms, as asserted.

Testing Procedure

The next step in applying of the method of moments is to select the testing procedure. As testing functions, we choose the expansion functions \bar{f}_n developed in the previous section. With the symmetric product definition

$$\langle \bar{f}, \bar{g} \rangle \equiv \int_S \bar{f} \cdot \bar{g} \, dS, \quad (10)$$

we test Eq. (5) with \bar{f}_m , yielding

$$\langle \bar{E}^1, \bar{f}_m \rangle = j\omega \langle \bar{A}, \bar{f}_m \rangle + \langle \nabla \Phi, \bar{f}_m \rangle. \quad (11)$$

By standard surface vector calculus formulas [19], the last term in (11) can be rewritten as

$$\langle \nabla \Phi, \bar{f}_m \rangle = - \int_S \Phi \nabla_s \cdot \bar{f}_m \, dS, \quad (12)$$

where use has been made of the fact that none of the \bar{f}_m has a component normal to any part of the boundary of S. Using (7), we next approximate the

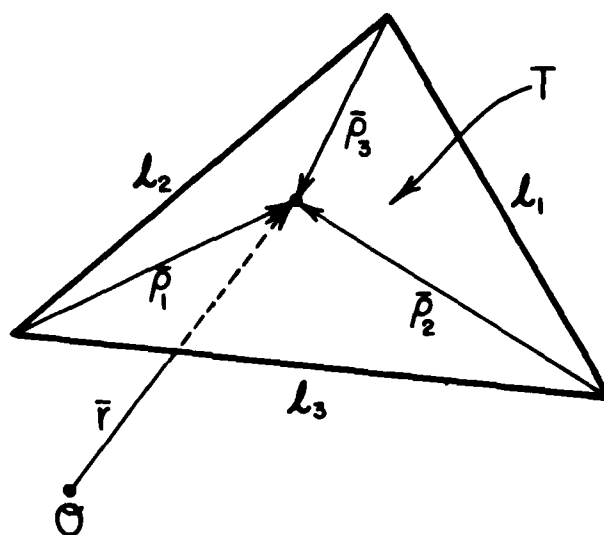


Fig. 5. Edges and local coordinates associated with a triangle.

integral in (12) as follows:

$$\begin{aligned} \int_S \Phi \nabla_s \cdot \bar{f}_m dS &= \ell_m \left(\frac{1}{A_m^+} \int_{T_m^+} \Phi dS - \frac{1}{A_m^-} \int_{T_m^-} \Phi dS \right) \\ &\approx \ell_m \left[\Phi(\bar{r}_m^{c+}) - \Phi(\bar{r}_m^{c-}) \right] \end{aligned} \quad (13)$$

where the two averages of Φ over triangles T_m^+ and T_m^- have been approximated by the corresponding values of Φ at the centroids of the triangles. We similarly approximate the integration of the vector potential and incident field terms in (11):

$$\begin{aligned} \left\langle \frac{\bar{E}^1}{\bar{A}} \right\rangle, \bar{f}_m &= \ell_m \left[\frac{1}{2A_m^+} \int_{T_m^+} \left\{ \frac{\bar{E}^1}{\bar{A}} \right\} \cdot \bar{\rho}_m^+ dS + \frac{1}{2A_m^-} \int_{T_m^-} \left\{ \frac{\bar{E}^1}{\bar{A}} \right\} \cdot \bar{\rho}_m^- dS \right] \\ &\approx \frac{\ell_m}{2} \left[\left\{ \frac{\bar{E}^1(\bar{r}_m^{c+})}{\bar{A}(\bar{r}_m^{c+})} \right\} \cdot \left(\bar{\rho}_m^{c+} \right) + \left\{ \frac{\bar{E}^1(\bar{r}_m^{c-})}{\bar{A}(\bar{r}_m^{c-})} \right\} \cdot \left(\bar{\rho}_m^{c-} \right) \right], \end{aligned} \quad (14)$$

where the integrals are eliminated by approximating \bar{E}^1 and \bar{A} with their values at the centroid of each triangle and then carrying out integrations similar to those used to obtain (8). With (12) - (14), (11) now becomes

$$\begin{aligned} j\omega \ell_m \left[\bar{A}(\bar{r}_m^{c+}) \cdot \frac{\bar{\rho}_m^{c+}}{2} + \bar{A}(\bar{r}_m^{c-}) \cdot \frac{\bar{\rho}_m^{c-}}{2} \right] &+ \ell_m \left[\Phi(\bar{r}_m^{c+}) - \Phi(\bar{r}_m^{c-}) \right] \\ &= \ell_m \left[\bar{E}^1(\bar{r}_m^{c+}) \cdot \frac{\bar{\rho}_m^{c+}}{2} + \bar{E}^1(\bar{r}_m^{c-}) \cdot \frac{\bar{\rho}_m^{c-}}{2} \right], \end{aligned} \quad (15)$$

which is the equation to be enforced at each triangle edge, $m = 1, 2, \dots, N$. Another interpretation of the testing procedure arriving at (15) is also possible. One may integrate the vector component of (5) parallel to the path from the point \bar{r}_m^{c+} to $(\bar{r}_m^{c+} + \bar{\rho}_m^{c+}/2)$ and thence to \bar{r}_m^{c-} , approximating \bar{E}^1 and \bar{A}^1

along each portion of the path by their respective values at the triangle centroids. The resulting equality, when multiplied by ℓ_m , is Eq. (15). Under either interpretation, the purpose of the testing procedure is reduce the differentiability requirement on Φ by integrating it first. The purpose of approximations (13) and (14) is to remove all surface integrals of potential quantities; were this not done, a prohibitively expensive two-fold surface integration would be required to fill the moment matrix since computation of the potentials themselves already involves one surface integration.

Evaluation of Matrix Elements

Substitution of the current expansion (9) into (15) yields an $N \times N$ system of linear equations which may be written in matrix form as

$$Z I = V \quad (16)$$

where $Z = [Z_{mn}]$ is an $N \times N$ matrix and $I = [I_n]$ and $V = [V_m]$ are column vectors of length N . Elements of Z and V are given by

$$Z_{mn} = \ell_m \left[j\omega \left(\bar{A}_{mn}^+ \cdot \frac{\bar{\rho}_m^{c+}}{2} + \bar{A}_{mn}^- \cdot \frac{\bar{\rho}_m^{c-}}{2} \right) + \phi_{mn}^+ - \phi_m^- \right] \quad (17)$$

$$V_m = \ell_m \left(\bar{E}_m^+ \cdot \frac{\bar{\rho}_m^{c+}}{2} + \bar{E}_m^- \cdot \frac{\bar{\rho}_m^{c-}}{2} \right) \quad (18)$$

where

$$\bar{A}_{mn}^\pm = \frac{\mu}{4\pi} \int_S \bar{f}_n(\bar{r}') \frac{e^{-jkR_m^\pm}}{R_m^\pm} dS', \quad (19)$$

$$\phi_{mn}^\pm = - \frac{1}{4\pi j\omega\epsilon} \int_S \nabla_s \cdot \bar{f}_n(\bar{r}') \frac{e^{-jkR_m^\pm}}{R_m^\pm} dS', \quad (20)$$

$$R_m^\pm = |\bar{r}_m^{c\pm} - \bar{r}'|$$

and

$$\bar{E}_m^\pm = \bar{E}^1(\bar{r}^{\pm c_m}). \quad (21)$$

For plane wave incidence, we set

$$\bar{E}^1(\bar{r}) = (E_\theta \hat{\theta}_0 + E_\phi \hat{\phi}_0) e^{j\bar{k} \cdot \bar{r}} \quad (22)$$

where the propagation vector \bar{k} is

$$\bar{k} = (k \sin \theta_0 \cos \phi_0 \hat{x} + k \sin \theta_0 \sin \phi_0 \hat{y} + k \cos \theta_0 \hat{z}) \quad (23)$$

and (θ_0, ϕ_0) defines the angle from which the plane wave arrives in the usual spherical coordinate convention. The unit vectors $\hat{\theta}_0$ and $\hat{\phi}_0$ are constant vectors which coincide with the spherical coordinate unit vectors at points on the line from 0 in the direction of \bar{k} . Once the matrices Z and V of (16) are determined, one may solve the system of linear equations for I .

We note that although a general matrix element Z_{mn} is associated with the pair of edges m and n , each computed integral appearing in Z_{mn} is actually related to a source triangle attached to edge n with an observation point at the centroid of a triangle attached to edge m . For each such observation and source triangle pair, these same integrals contribute to an element of Z whose row index corresponds to one of the observation triangle edges and whose column index corresponds to one of the source triangle edges. Thus, rather than individually compute each element of Z_{mn} , we instead compute all vector and scalar potentials associated with each observation- and source-face combination and then place the quantities, appropriately weighted, into the elements of Z corresponding to the various edges associated with these faces. (The face matrix described in Appendix A provides a convenient means for keeping track of the correspondence between faces and

edges as well as for determining the current reference directions within each patch.) Doing the computations in this fashion results in up to a nine-fold increase in efficiency in filling the matrix Z over the direct edge-by-edge approach.

In accordance with the above discussion, let us consider the evaluation of the vector and scalar potential integrals for a given source and observation face combination. Fig. 6 illustrates an observation point in face p with current sources residing in face q . For purposes of illustration, we assume the edges of face q are numbered 1, 2, and 3 with edge lengths ℓ_1 , ℓ_2 , and ℓ_3 , and opposite vertices at \bar{r}_1 , \bar{r}_2 , and \bar{r}_3 , respectively. We further denote face q simply as triangle T^q with area A^q . Each of the three basis functions which may exist simultaneously in T is proportional to one of the vectors $\bar{\rho}_1$, $\bar{\rho}_2$, and $\bar{\rho}_3$ defined in Fig. 6, where the subscripts correspond to the associated edges and we have dropped the \pm superscripts. Each of the vectors $\bar{\rho}_i$, $i = 1, 2, 3$, is shown directed away from its associated vertex in the figure, but may instead be directed toward the vertex if the current reference direction for that edge is into the triangle. Consequently,

$$\bar{\rho}_i = \pm (\bar{r}' - \bar{r}_i), \quad i = 1, 2, 3, \quad (24)$$

where the positive sign is used if the positive current reference direction is out of T^q and the negative sign is used otherwise. We wish to evaluate the magnetic vector potential,

$$\bar{A}_1^{pq} = \frac{\mu}{4\pi} \int_{T^q} \left(\frac{\ell_i}{2A^q} \right) \bar{\rho}_i \frac{e^{-jkR^p}}{R^p} ds', \quad (25)$$

and electric scalar potential,

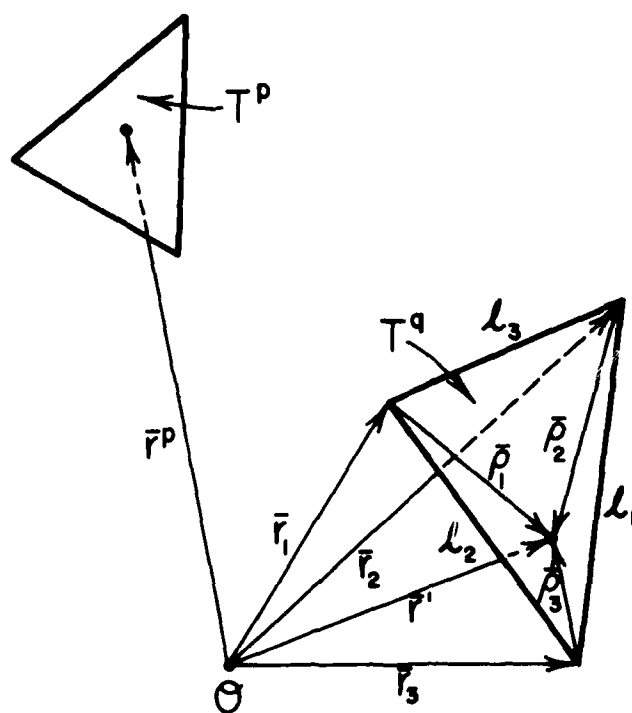


Fig. 6. Local coördinates and edges for source triangle T^q with observation point in triangle T^p .

$$\phi_1^{pq} = \frac{1}{4\pi\epsilon} \int_{T^q} \left(\frac{\rho_1}{A^q} \right) \frac{e^{-jkR^p}}{R^p} dS', \quad (26)$$

associated with the 1^{th} basis function on face q observed at the centroid of face p . In (25) and (26),

$$R^p = |\bar{r}^{cp} - \bar{r}'| \quad (27)$$

where \bar{r}^{cp} is the position vector of the centroid of face p .

Integrals (25) and (26) are most conveniently evaluated by transforming to area coordinates [20] within the source triangle. Fig. 7 shows the position vector \bar{r}' at some arbitrary point in T^q . The vectors $\bar{\rho}_i$ then divide T^q into three regions of areas A_1 , A_2 , and A_3 which are constrained to satisfy $A_1 + A_2 + A_3 = A^q$. We define the normalized area coordinates as

$$\xi = \frac{A_1}{A^q}, \quad (28a)$$

$$\eta = \frac{A_2}{A^q}, \quad (28b)$$

$$\zeta = \frac{A_3}{A^q}, \quad (28c)$$

which, because of the area constraint, must satisfy

$$\xi + \eta + \zeta = 1. \quad (29)$$

Note that all three coordinates vary between zero and unity in T^q and that at the triangle corners, \bar{r}_1 , \bar{r}_2 , and \bar{r}_3 , the triplet (ξ, η, ζ) takes on the values $(1,0,0)$, $(0,1,0)$, and $(0,0,1)$, respectively. The transformation from Cartesian to area coordinates may be written in vector form as

$$\bar{r}' = \xi \bar{r}_1 + \eta \bar{r}_2 + \zeta \bar{r}_3, \quad (30)$$

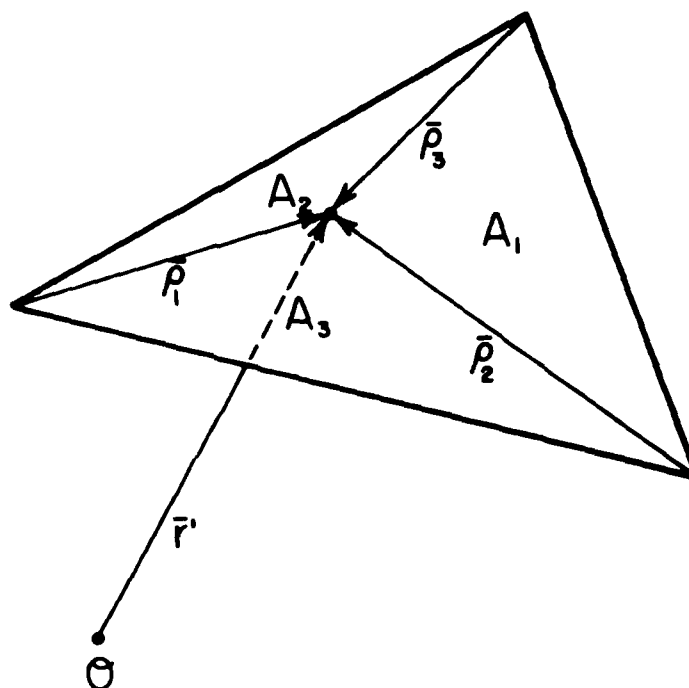


Fig. 7. Definitions of areas used in defining area coordinates.

where ξ , η , and ζ are subject to the constraint (29). It can easily be shown that surface integrals over T^q transform as follows:

$$\int_{T^q} g(\bar{r}) dS = 2A^q \int_0^1 \int_0^{1-\eta} g(\xi \bar{r}_1 + \eta \bar{r}_2 + (1-\xi-\eta)\bar{r}_3) d\xi d\eta. \quad (31)$$

With (24), (27), (30), and (31), (25) and (26) may now be written as

$$\bar{A}_i^{pq} = \pm \frac{\mu \ell_i}{4\pi} (\bar{r}_1 I_{\xi}^{pq} + \bar{r}_2 I_{\eta}^{pq} + \bar{r}_3 I_{\zeta}^{pq} - \bar{r}_i I^{pq}) \quad (32)$$

and

$$\phi_i^{pq} = \mp \frac{\ell_i}{j2\pi\omega\epsilon} I^{pq}, \quad (33)$$

where

$$I^{pq} = \int_0^1 \int_0^{1-\eta} \frac{e^{-jkR^p}}{R^p} d\xi d\eta, \quad (34a)$$

$$I_{\xi}^{pq} = \int_0^1 \int_0^{1-\eta} \xi \frac{e^{-jkR^p}}{R^p} d\xi d\eta, \quad (34b)$$

$$I_{\eta}^{pq} = \int_0^1 \int_0^{1-\eta} \eta \frac{e^{-jkR^p}}{R^p} d\xi d\eta, \quad (34c)$$

$$I_{\zeta}^{pq} = I^{pq} - I_{\xi}^{pq} - I_{\eta}^{pq}. \quad (34d)$$

Thus we see that only three independent integrals, (34a) - (34c), must be numerically evaluated for each combination of face pairs p and q . The three integrals, in turn, contribute to up to nine elements of Z in (17). For a closed object, the number of independent integrals to be computed turns out to be $(4/3) N^2$. Numerical evaluation of the integrals (34a) - (34c) may be accomplished by using numerical quadrature techniques specially developed for

triangular domains [21] together with the procedures discussed in Appendix B.

III. MAGNETIC FIELD FORMULATION

In this section, the magnetic field integral equation (MFIE) is derived for a conducting scatterer S . Since the MFIE applies only to closed bodies, throughout this section we assume that S has no boundary edges. The vector basis functions \bar{f}_n of the previous section, used there as expansion and testing functions for the EFIE, are chosen to play the same roles here in the numerical solution of the MFIE. The resulting moment matrix elements are given and their numerical evaluation is also discussed in this section.

Magnetic Field Integral Equation

The magnetic field integral equation is derived by noting that the induced current \bar{J} on S is related to the incident and scattered magnetic fields \bar{H}^i and \bar{H}^s , respectively, by

$$\bar{J} = \hat{n} \times (\bar{H}^i + \bar{H}^s), \quad (35)$$

where \hat{n} is an outward unit normal vector on S . It may be shown by a detailed limiting argument [19] that for observation points \bar{r} not on an edge,

$$\begin{aligned} \hat{n} \times \bar{H}^s &= \lim_{\bar{r} \rightarrow S} \hat{n} \times \nabla \times \bar{A} \\ &= \frac{\bar{J}}{2} + \hat{n} \times \frac{1}{4\pi} \int_S \bar{J} \times \nabla' G dS', \end{aligned} \quad (36)$$

where $G = \exp(-jkR)/R$ and \bar{r} approaches S from the exterior. Combining (35) and (36), we obtain the magnetic field integral equation (MFIE):

$$\hat{n} \times \bar{H}^1 = \frac{\bar{J}}{2} - \hat{n} \times \frac{1}{4\pi} \int_S \bar{J} \times \nabla' G dS'. \quad (37)$$

Eq. (37) is an integral equation of the second kind (i.e., the unknown \bar{J} appears outside as well as under the integral), and the kernel is regular. In fact, if S is a triangulated surface and \bar{r} is some point on S interior to a planar triangular face, then the current in that face does not contribute to the integral since $\bar{J} \times (\bar{r} - \bar{r}')$ is parallel to \hat{n} there. A slight modification to (36) and (37) is required if \bar{r} is directly on an edge [22]; this situation will not arise in the present approach, however.

Expansion and Testing Procedure

As with the EFIE, we find the functions \bar{f}_n to be suitable both as expansion and testing functions. Treating the testing procedure first, we test (37) with \bar{f}_n and use approximations paralleling those yielding (13) and (14) to obtain

$$\begin{aligned} \ell_m \left[\hat{n}_m^+ \times \bar{H}^1(\bar{r}_m^{c+}) \cdot \frac{\bar{\rho}_m^{c+}}{2} + \hat{n}_m^- \times \bar{H}^1(\bar{r}_m^{c-}) \cdot \frac{\bar{\rho}_m^{c-}}{2} \right] \\ = \frac{1}{2} \langle \bar{J}, \bar{f}_m \rangle - \ell_m \left[\frac{\bar{\rho}_m^{c+}}{2} \cdot \hat{n}_m^+ \times \frac{1}{4\pi} \int_S \bar{J} \times (\nabla' G)_m^+ dS' \right. \\ \left. + \frac{\bar{\rho}_m^{c-}}{2} \cdot \hat{n}_m^- \times \frac{1}{4\pi} \int_S \bar{J} \times (\nabla' G)_m^- dS' \right] \end{aligned} \quad (38)$$

where \hat{n}_m^+ is the outward surface normal in triangle T_m^+ and

$$(\nabla' G)_m^\pm = (\bar{r}_m^{c\pm} - \bar{r}') (1 + jkR_m^\pm) \exp(-jkR_m^\pm) / (R_m^\pm)^3. \quad \text{Substituting expansion (9)}$$

for \bar{J} results in a matrix equation of the form

$$\beta I = I^1, \quad (39)$$

where the elements of the matrix $\beta = [\beta_{mn}]$ and the column vector $I^i = [I_m^i]$ are given by

$$\beta_{mn} = \frac{1}{2} \langle \bar{f}_m, \bar{f}_n \rangle - \ell_m \left[\frac{\bar{\rho}_m^{c+}}{2} \cdot \hat{n}_m^+ \times \frac{1}{4\pi} \int_S \bar{f}_n \times (\nabla' G)_m^+ dS' + \frac{\bar{\rho}_m^{c-}}{2} \cdot \hat{n}_m^- \times \frac{1}{4\pi} \int_S \bar{f}_n \times (\nabla' G)_m^- dS' \right] \quad (40)$$

and

$$I_m^i = \ell_m \left[\hat{n}_m^+ \times \bar{H}^i(\bar{r}_m^{c+}) \cdot \frac{\bar{\rho}_m^{c+}}{2} + \hat{n}_m^- \times \bar{H}^i(\bar{r}_m^{c-}) \cdot \frac{\bar{\rho}_m^{c-}}{2} \right]. \quad (41)$$

Solution of (39) yields the column vector I of coefficients of the current expansion.

Evaluation of Matrix Elements

One notes that a matrix element β_{mn} is associated with edge pair m and n of S , whereas the integrals and observation points appearing on β_{mn} in (40) are associated with the faces that are connected to edges m and n . Consequently, it is efficient, as with the EFIE, to evaluate all integrals required for a given face-face combination and then to sort the integrals into the appropriate rows and columns of β with the aid of the face matrix (Appendix A), which provides a mapping from faces to edges.

Referring to Fig. 6 and the analysis following (24), we may write the required integrals in terms of the vector integral

$$\bar{I}_1^{pq} = \frac{1}{4\pi} \int_{T^q} \left(\frac{\ell_1}{2A^q} \right) \bar{\rho}_1 \times (\bar{r}^{cp} - \bar{r}') (1 + jkR^p) \frac{e^{-jkR^p}}{(R^p)^3} dS', \quad p \neq q, \quad (42)$$

which represents the contribution at the centroid of the p^{th} triangle due to the i^{th} basis function ($i = 1, 2, 3$) in triangle q . If $p=q$, $\bar{I}_i^{pq} = 0$. Eq. (42) can be written in terms of area coordinates defined on T^q as

$$\bar{I}_i^{pq} = \frac{\ell_i}{4\pi} [(\bar{r}^{cp} \times \bar{r}_i) J^{pq} + (\bar{r}_i - \bar{r}^{cp}) \times (\bar{r}_1 J_\xi^{pq} + \bar{r}_2 J_\eta^{pq} + \bar{r}_3 J_\zeta^{pq})], \quad p \neq q, \quad (43)$$

where

$$J^{pq} = \int_0^1 \int_0^{1-\eta} (1+jkR^p) \frac{e^{-jkR^p}}{(R^p)^3} d\xi d\eta \quad (44a)$$

$$J_\xi^{pq} = \int_0^1 \int_0^{1-\eta} \xi (1+jkR^p) \frac{e^{-jkR^p}}{(R^p)^3} d\xi d\eta \quad (44b)$$

$$J_\eta^{pq} = \int_0^1 \int_0^{1-\eta} \eta (1+jkR^p) \frac{e^{-jkR^p}}{(R^p)^3} d\xi d\eta \quad (44c)$$

$$J_\zeta^{pq} = J^{pq} - J_\xi^{pq} - J_\eta^{pq} \quad (44d)$$

and R is given by (27). The evaluation of (44a) - (44c) may be accomplished by numerical quadrature by the method of [21].

We next consider the evaluation of contributions from each patch to the symmetric product term in (40). If edges m and n do not lie on a common triangle, there is no contribution to the symmetric product. If they lie on a common triangle T^q , then let us assume for illustration that $m, n = 1, 2$, or 3 as in Fig. 6. Then the contribution from T^q to the symmetric product is

$$\frac{1}{2} \left\langle \frac{\ell_m}{A^q} \bar{\rho}_m, \frac{\ell_n}{A^q} \bar{\rho}_n \right\rangle_{T^q} \equiv \pm \frac{\ell_m \ell_n}{2(A^q)^2} \int_{T^q} \bar{\rho}_m \cdot \bar{\rho}_n dS'$$

$$= \pm \frac{\ell_m \ell_n}{8(A^q)^2} \left[\frac{3|\bar{r}^{cq}|^2}{4} + \frac{|\bar{r}_1|^2 + |\bar{r}_2|^2 + |\bar{r}_3|^2}{12} - (\bar{r}_m + \bar{r}_n) \cdot \bar{r}^{cq} + \bar{r}_m \cdot \bar{r}_n \right] \quad (45)$$

where the positive sign is selected if the reference directions of edges m and n are both directed either into or out of T^q ; the negative sign is selected otherwise. If $m=n$, two terms of the form of (45) contribute to β_{mn} , one from T_m^+ and one from T_m^- .

IV. NUMERICAL RESULTS

In this section, numerical results are presented for current distributions induced on selected scatterers under plane wave illumination. The geometries considered are a conducting square plate, a bent plate, a circular disk, and a sphere. The first three of these involve open surfaces and therefore test the EFIE approach when edges are present. The disk is also an example of a structure whose curved boundary is not amenable to modeling by rectangular patches, and the sphere is both an example of a closed surface, to which both the EFIE and MFIE apply, and of a doubly-curved surface, which is not amenable to rectangular patch modeling.

Flat Plate

Fig. 8 and 9 show the dominant component current distributions along the two principal cuts on a square plate illuminated by a normally incident plane wave. For comparison, the solution of Glisson [18], obtained using rectang-

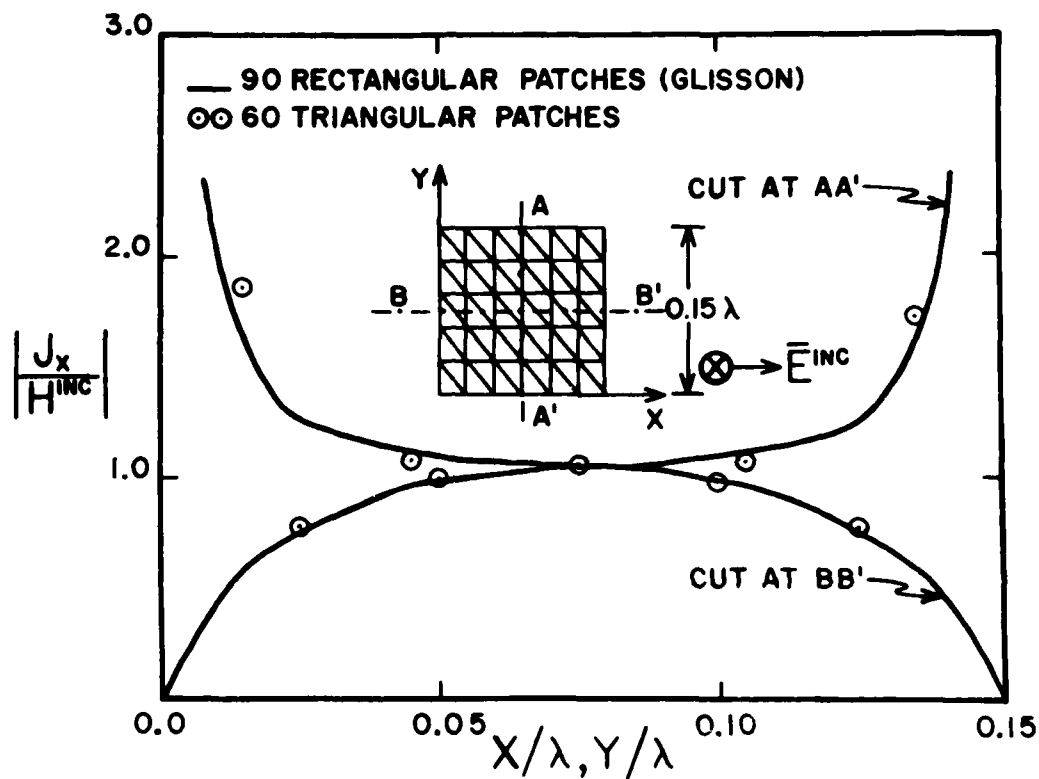


Fig. 8. Distribution of dominant component of current on 0.15λ square flat plate.

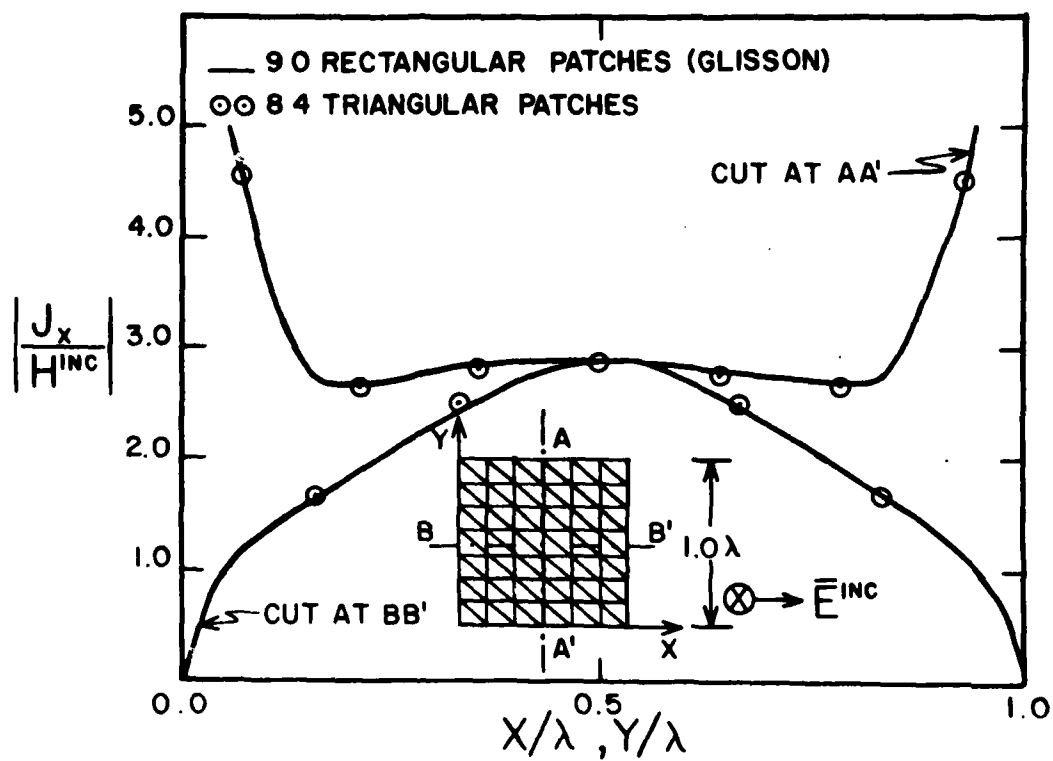


Fig. 9. Distribution of dominant component of current on a 1.0λ square flat plate.

ular patches, is also given. The number of patches listed in the figures refers to the number of charge patches in the earlier solution of Glisson and to the number of triangles (also equal to the number of charge patches) in the present solution. Note that these quantities play similar roles in the two approaches. No comparison of the rate of convergence of the two approaches should be inferred from the figures since both solutions are already well-converged for the number of unknowns used. Note also that the density of data points appearing in the figures for the triangular patch solution is not truly indicative of the linear density of the subdomains. This is because, in effect, we show data points for every other edge, i.e. only for those edges where the associated current normal to the edge is parallel to the current component we wish to observe.

Fig. 8 shows the current induced on a plate 0.15λ on each side. At this low frequency, the current distribution is largely determined by the edge conditions and this case therefore provides a good test of the method's ability to handle surface edges. We note the absence of any anomalies in the computed distribution near the plate edges. The elimination of such anomalies is attributed to using basis functions in which the expansion coefficients are not associated with currents at plate edges and to a testing procedure in which potentials are not evaluated at edges [15].

Fig. 9 shows corresponding results for a 1.0λ square plate. It also shows that the edge behavior of the current distribution is confined to a smaller region near the edges than for the 0.15λ plate and that the current on the interior portion of the plate is beginning to exhibit the physical optics-plus-standing wave distribution characteristic of the higher frequencies.

Bent Plate

Figs. 10 and 11 show the dominant component current distributions along the center and perpendicular to the direction of current flow at two frequencies on a square plate bent through an angle of 50° . The bend is located at a distance of one-third the plate width from an edge and a plane wave with the electric field polarized parallel to the bend is incident normal to the larger section of the bent plate. Other polarizations and angles of incidence have been examined and the resulting current distributions show good correspondence with those of Glisson [18].

Circular Disk

Fig. 12 shows the computed current distribution on a circular disk illuminated by a normally incident plane wave. The component J_ϕ is shown along the cut across the diameter oriented perpendicular to the incident electric field vector. Also shown for comparison is the quasi-static solution valid at low frequencies [23].

Sphere

Fig. 13 shows the current distribution computed by the EFIE along the principal cuts on a 0.2λ radius conducting sphere. The cases of axial incidence and equatorial incidence are both considered in order to observe the influence of the triangulation scheme on the solution. Also shown for comparison is the exact eigenfunction solution. Both illuminations show very good agreement with the exact solution.

Since the sphere is a closed body, this problem may also be examined using the MFIE. Fig. 14 shows the results of the MFIE computation. Comparison of the exact solution with the MFIE computation is disappointing, partic-

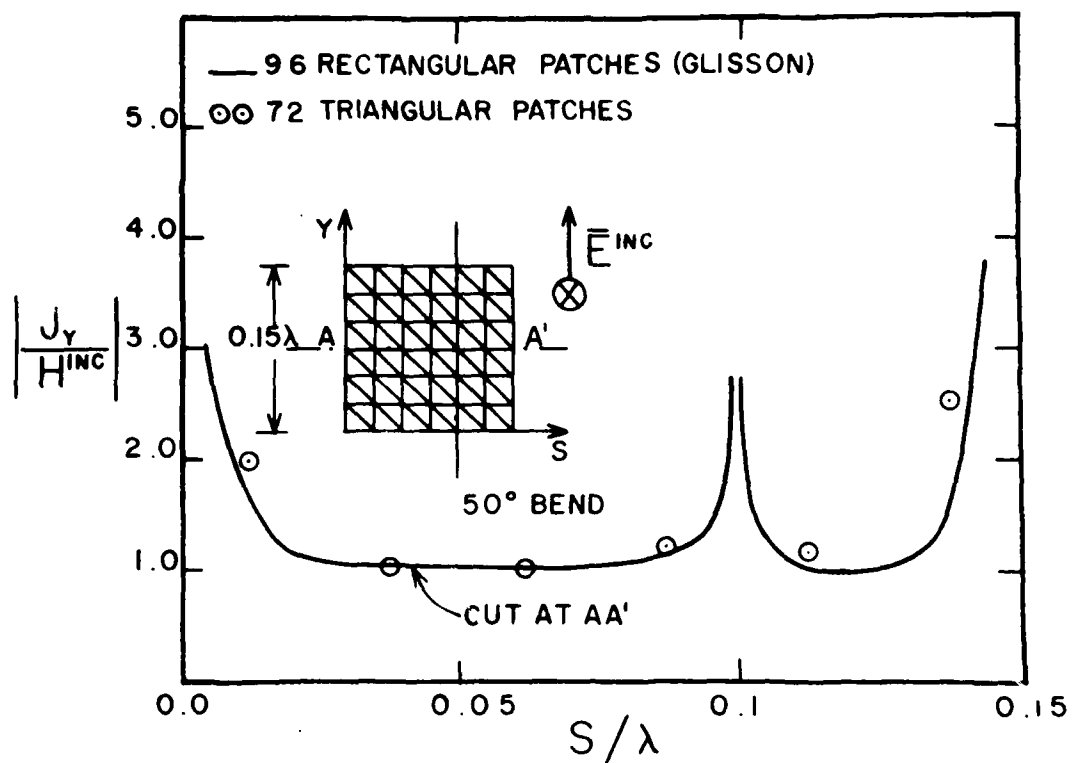


Fig. 10. Distribution of dominant component of current on a 0.15λ bent square plate.

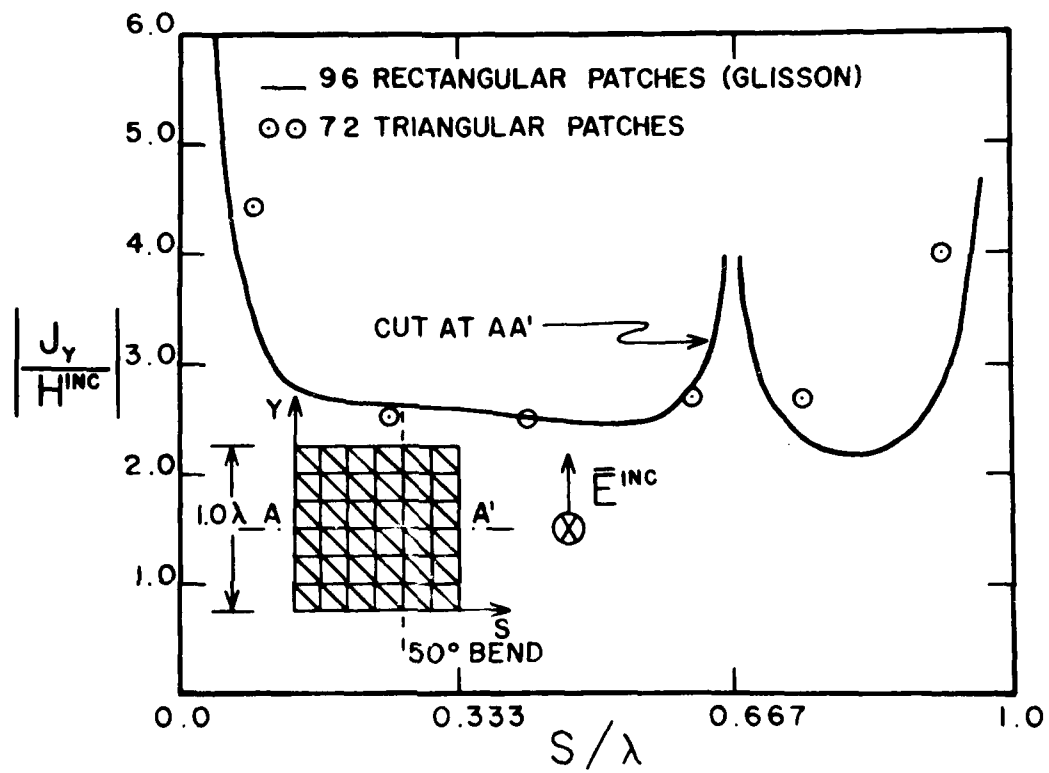


Fig. 11. Distribution of dominant component of current on a 1.0λ bent square plate.

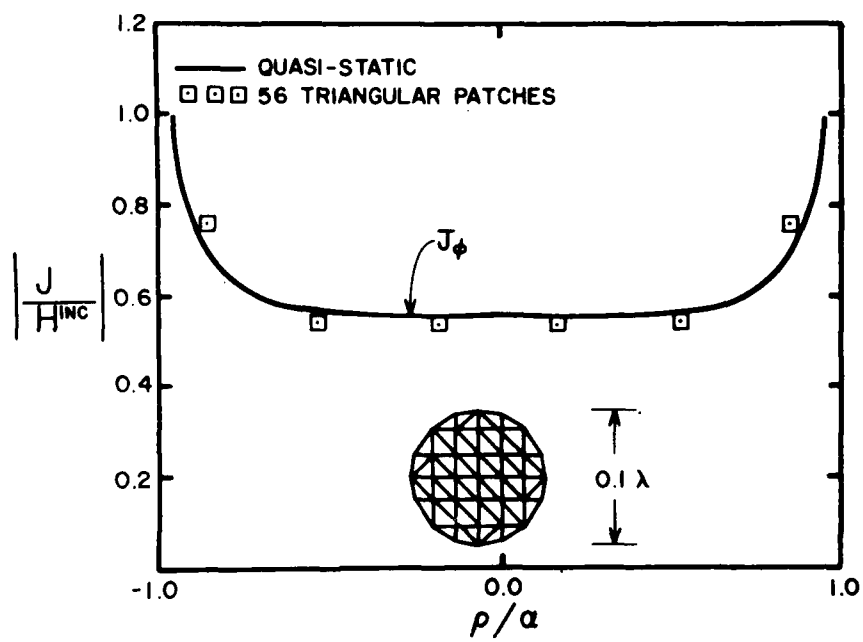


Fig. 12. Distribution of current on a 0.05λ radius circular disk.

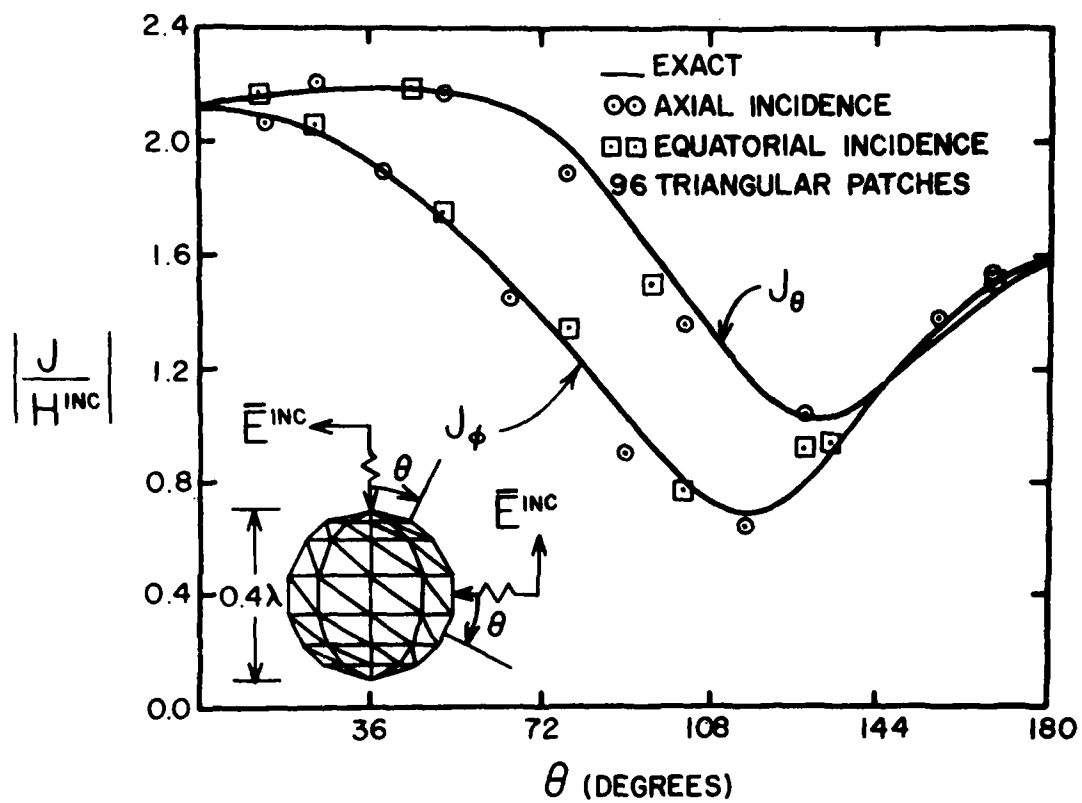


Fig. 13. Distribution of current components on a 0.2λ radius conducting sphere calculated by an electric field integral equation formulation.

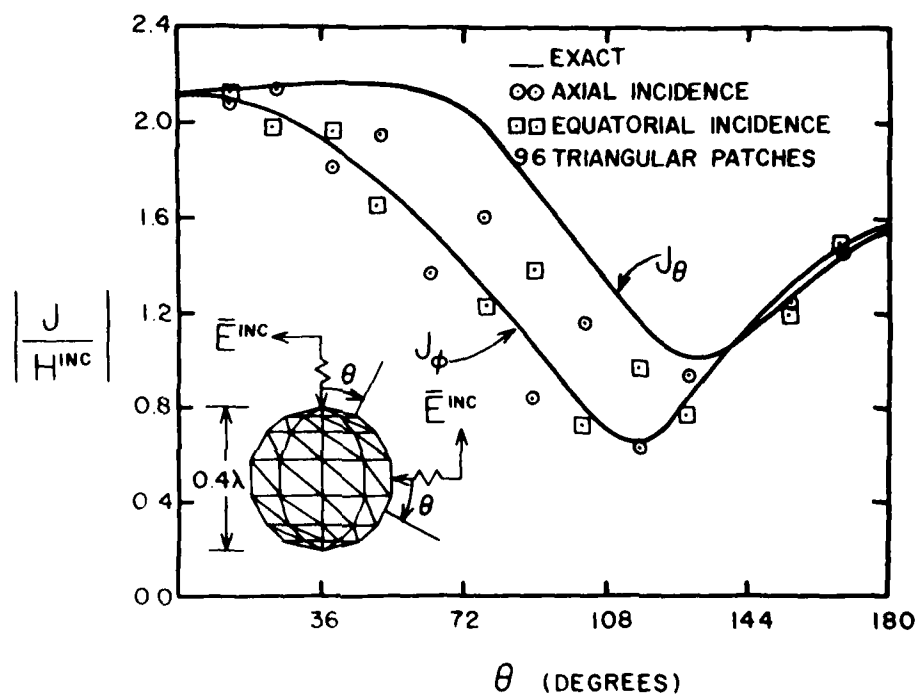


Fig. 14. Distribution of current components on a 0.2λ radius conducting sphere calculated by a magnetic field integral equation formulation.

ularly when compared with the EFIE solution. In an attempt to try to improve the accuracy of the MFIE, an alternative testing procedure was also examined in which point-matching at the mid-points of edges was used. Although this had the effect of radically changing several of the elements, including the diagonal, of the matrix, the resultant current distributions were virtually indistinguishable from Fig. 14 . Due to computer budget limitations, further experimentation with frequency, number of unknowns, and triangulation schemes was not possible. We point out, however, that the surface discretization used results in a rather crude approximation to the sphere and we suggest that perhaps the good agreement in the EFIE case may have been largely fortuitous. More experimentation is obviously needed to establish the superiority of either formulation for closed bodies.

V. SUMMARY

In this report, the electric field integral equation (EFIE) is used with the moment method to develop a simple and efficient numerical procedure for treating problems of scattering by arbitrarily-shaped objects. The objects are modeled for numerical purposes by planar triangular surface patch models. Because the EFIE formulation is used, the procedure is applicable to both open and closed bodies. Crucial to the formulation is the development of a set of special subdomain basis functions defined on pairs of adjacent triangular patches. The basis functions yield a current representation which is free of line or point charges at subdomain boundaries.

A second approach using the magnetic field integral equation (MFIE) and employing the same basis functions is also developed. Although the MFIE applies only to closed bodies, the moment matrix of the MFIE is also needed in dielectric scattering problems and in the so-called combined field integral equation used to eliminate difficulties with internal resonances present in the MFIE and EFIE formulations.

The EFIE approach is applied to the scattering problems of plane wave illumination of a flat square plate, a bent square plate, a circular disk, and a sphere. Comparisons of surface current densities are made with previous computations or exact formulations and good agreement is obtained in each case. The MFIE approach is also applied to the sphere and reasonable agreement with exact calculations is obtained.

APPENDIX A

TOPOLOGICAL PROPERTIES AND MATHEMATICAL REPRESENTATION OF TRIANGULATED SURFACES

In this appendix we consider some topological properties of a triangulated surface and present a simple mathematical representation for such a surface. In the topological discussion a number of geometrical quantities are defined and some relationships between them are given. Consideration is then given to a means for mathematically representing a triangulated surface in a form that is convenient whether the surface data is supplied by the modeler or is generated by an automatic surface triangulation computer subprogram [24]. From this representation may be derived an alternative representation which is actually more convenient for the subsequent numerical processing necessary in applying the moment method.

We mention here at the outset that one aspect of the electrical representation of the scattering problem also has a bearing on what information is required in the geometrical representation of the surface. That factor is that the unknowns to be solved for are the components of current normal to each triangle edge. There are two possible senses in which the current can flow normal to each edge and the modeler should be able to select either choice to establish an assumed reference direction for the current at each edge. Furthermore, it is desirable that the reference current specification be incorporated, if possible, in the geometrical representation so as to

minimize the amount of user-supplied data. As will be seen, the geometrical representation given here does indeed incorporate the specification of current reference directions.

An arbitrary body modeled by triangular patches is shown in Fig. A1. The body is assumed to be connected, orientable, of finite extent, and composed of non-intersecting surfaces. In general, a triangulated surface modeling an arbitrary body consists of N_f planar triangular faces, N_v vertices, and N_e edges. These geometrical elements are illustrated in Fig. A1.

An arbitrary surface may also have N_h handles. Roughly speaking, a handle is a portion of a surface which, if detached from the surface, would resemble a torus (Fig. A1). Any closed, orientable surface with N_h handles may be continuously deformed, by twisting and stretching, into a sphere with N_h handles. These spheres with N_h handles may be thought of as canonical objects used to classify all closed, orientable surfaces. In deforming surfaces into spheres with handles, edges are permitted to pass through one another, but they may not be broken or disconnected. A surface with no handles is simply-connected; a surface with N_h handles is said to be $(N_h + 1)$ -connected.

If a surface is open, it is bounded by one or more boundary curves (Fig. A1), each of which is assumed to form a closed, non-intersecting curve on the surface. We may associate with each boundary curve an aperture, which is any simply-connected surface having one and only one boundary curve congruent to the associated boundary curve on the triangulated surface.

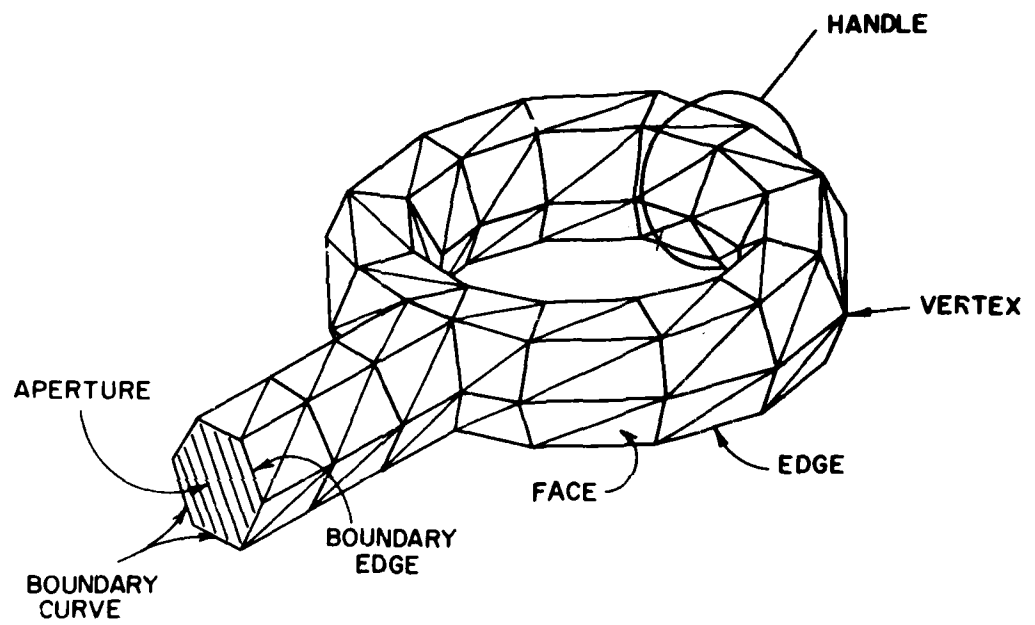


Fig. A1. Arbitrary surface modeled by triangular patches.

Intuitively, an aperture surface is merely a surface which can be used to cover a "hole" in another surface. (Unfortunately, the term "hole" is not appropriate to describe regions such as that exterior to the boundary curve of a rectangular plate, and hence we use the term "aperture" to describe a closing surface instead. For the rectangular plate, for example, a suitable aperture is a rectangular box with one open end.) We assume that an arbitrary surface has N_a apertures (and associated boundary curves) and that a total of N_b edges, called boundary edges, lie on these boundary curves. If there are no boundary edges, $N_b=0$ and the surface is closed.

We next employ a theorem due to Euler which states that [25] for closed surfaces,

$$N'_f - N'_e + N'_v = 2(1-N_h). \quad (A1)$$

The primes remind us that the result applies only to closed surfaces. The right hand side of (A1) is a topological invariant known as the Euler characteristic and is the same for any closed surface which can be continuously deformed into a sphere with N_h handles. To extend the theorem to open surfaces, we first close all the apertures. This may be accomplished by introducing for each aperture an auxiliary vertex and auxiliary edges connected between this vertex and each vertex on the associated boundary contour (Fig. A2). These auxiliary vertices may be arbitrarily located, provided they do not coincide with one another or rest on edges or vertices of the original surface. The resulting closed triangulated surface consists of $N'_f = N_f + N_b$ faces, $N'_e = N_e + N_b$ edges, and $N'_v = N_v + N_a$ vertices. Substituting these relationships into (A1), one obtains

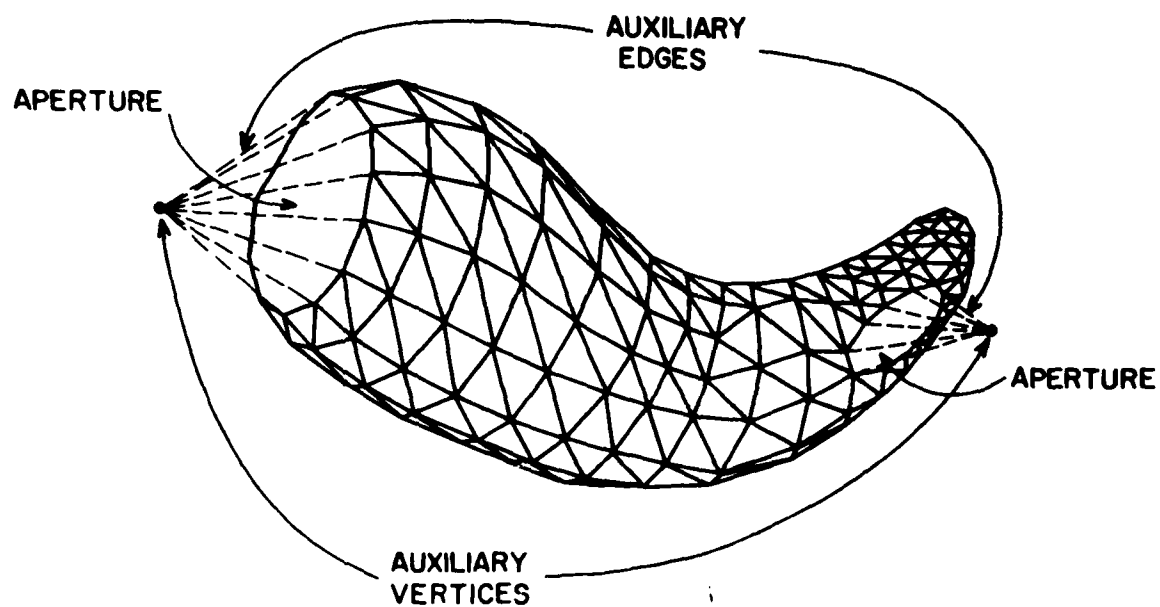


Fig. A2. Auxiliary vertices and edges used to close apertures to form a closed body.

$$N_f - N_e + N_v = 2(1 - N_h) - N_a, \quad (A2)$$

an extension of (A1) to open bodies. We may also eliminate either N_f or N_e in (A2) by noting that since all of the faces are triangular, $3N'_f = 2N'_e$. This follows from the fact that for a closed surface, each edge is counted twice if we sum the three edges per triangle over all the triangles. Use of this relation to eliminate N_f and N_e , respectively, in Eq. (A2) yields

$$N_e = 3N_v + 3N_a + 6(N_h - 1) - N_b \quad (A3)$$

and

$$N_f = 2N_v + 2N_a + 4(N_h - 1) - N_b. \quad (A4)$$

Eq. (A3) may be used to determine the number of unknowns to be found if one knows the number of vertices, apertures, handles, and boundary edges of the model. Since currents normal to boundary edges are zero and hence are not solved for, the number of unknowns, N , is equal to the number of surface interior edges, $N_e - N_b$.

A computer subroutine, GEOM, has been developed to accept data describing a triangulated surface and to generate auxiliary information and data necessary for further numerical processing. The subroutine requires two sets of input data. The first is an indexed list or vertex matrix of position vectors $\vec{r}_i = (x_i, y_i, z_i)$, $i = 1, 2, \dots, N_v$. The components of the vectors \vec{r}_i are the Cartesian coordinates of the i^{th} vertex with respect to a global coordinate system. The second set of data is an edge matrix

$$E = [e_{ij}], \quad i = 1, 2, \dots, N_e; \quad j = 1, 2 \quad (A5)$$

in which is listed in the i^{th} row the indices of the two vertices to which the i^{th} edge is connected. The order of appearance of the vertex indices

in each row of E assigns a vector direction to each edge, with the first index corresponding to the tail and the second, to the head of the vector. The cross-product of this vector with the surface normal of a face adjacent to the edge then gives a positive reference direction for the surface current in that face. GEOM does not actually compute surface normals to determine the reference directions, but uses a procedure to be discussed later.

The vertex and edge matrices together completely determine the surface geometry, the interconnections of the edges to form triangles, and the current reference directions. However, one notes that in filling the moment matrix, one integrates over the surface faces and that the results of the integrations must be placed in rows and columns of the moment matrix corresponding to the appropriate edges. Hence it is convenient to introduce a face matrix,

$$F = [f_{ij}], \quad i = 1, 2, \dots, N_f; \quad j = 1, 2, 3, \quad (A6)$$

relating edges to the corresponding faces. The i^{th} row of the face matrix contains the edge numbers of those edges making up the boundary of the i^{th} face. Subroutine GEOM makes use of information in the edge matrix to find each face, to assign it an index, and to fill out the corresponding row of the face matrix. The order in which the numbered edges appear in each row may be used to assign an orientation to the boundary curve formed by the edges of each face. We may associate this orientation, in turn, with the direction of the surface normal of each face through the usual convention relating a surface normal to an oriented boundary contour. If the surface normals for all the faces are to be on the same side of the

surface (which is always possible if the surface is orientable), then if one travels in the prescribed direction around the boundaries of two adjacent faces he must traverse their common edge in opposite directions (Fig. A3). GEOM makes use of this property to correctly order the elements in the face matrix so that the orientation of all the face normals is toward the same side of the surface. The direction of the surface normal is initially chosen by locating the lowest numbered edge connected to edge $i = 1$. Then these two edges are treated as vectors pointing away from their common vertex and their cross-product is computed with edge $i = 1$ as the second vector in the product. The surface normal is then assumed to be parallel to this cross-product. Thus, by properly numbering the edges connected to edge $i = 1$, the modeler can fix the choice of the normal for an open surface. Furthermore, as already noted, by properly ordering the elements of the edge matrix, he may also choose the positive reference direction for each individual edge.

If the surface is closed ($N_b = 0$), the normal pointing into the region exterior to the surface should always be chosen. In this case, GEOM automatically determines whether the correct choice has been made by calculating the volume of the model according to

$$\begin{aligned}
 V &= \int_V dV = \int_V \nabla \cdot (x\hat{x}) dV \\
 &= \int_S x\hat{x} \cdot \hat{n} dA = \int_S x n_x dA \\
 &= \sum_{i=1}^{N_f} n_x^i \int_{T^i} x dA
 \end{aligned}$$

$$= \sum_{i=1}^{N_f} n_x^i x_c^i A^i, \quad (A7)$$

where T^i is the triangular patch formed by the i^{th} face, n_x^i is the x-component of the normal to T^i , x_c^i is the x-coordinate of the centroid of T^i with respect to the global coordinate system, and A^i is the area of T^i . If the volume computed from Eq. (A7) turns out to be negative, then the modeler has erroneously chosen the interior normal and GEOM rectifies this by interchanging the first two elements in every row of the face matrix. The orientation information is used in subsequent calculations in the following way: If the boundary of a face and one of its edges have the same orientation (as determined by the face and edge matrix, respectively), then the positive reference direction for the current normal to the edge is out of the face. Otherwise, the reference direction is into the face (see Fig. A3).

In the course of computing the face matrix, GEOM also determines all boundary edges. It also sorts them into their corresponding boundary curves and hence determines how many apertures are present. Then using Eq. (A2), it determines how many handles the surface has and computes the number of interior edges (i.e., the number of unknown current coefficients) by $N = N_e - N_b$. Finally, as a partial check on the correctness of the triangulation scheme, GEOM checks to see if (A3) and (A4) are satisfied. This test would fail, for example, if through an error in an entry in the connection matrix a patch was not triangular, but quadrilateral.

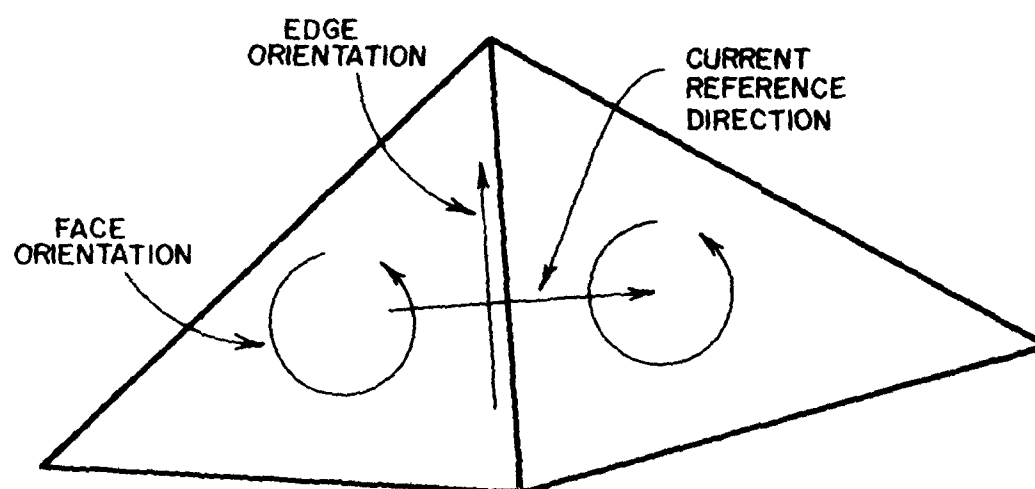


Fig. A3. Relationship between face and edge orientations and current reference direction at an edge.

APPENDIX B

EVALUATION OF INTEGRALS APPEARING IN THE ELECTRIC FIELD FORMULATION

In the solution of the EFIE using triangular patches, the numerical evaluation of the following three integrals is required:

$$I = \int_{\eta=0}^1 \int_{\xi=0}^{1-\eta} \frac{e^{-jkR}}{R} d\xi d\eta, \quad (B1)$$

$$I_{\xi} = \int_{\eta=0}^1 \int_{\xi=0}^{1-\eta} \xi \frac{e^{-jkR}}{R} d\xi d\eta, \quad (B2)$$

and

$$I_{\eta} = \int_{\eta=0}^1 \int_{\xi=0}^{1-\eta} \eta \frac{e^{-jkR}}{R} d\xi d\eta, \quad (B3)$$

where $R = |\bar{r} - \bar{r}'|$ and \bar{r}' is a position vector within a triangle whose area coordinates are ξ and η . If the observation point \bar{r} is within the triangle, then R will be zero for some value of ξ and η and the integrands of all three integrals will be singular. To circumvent difficulties with this case, we rewrite (B1) - (B3) as

$$I = \int_{\eta=0}^1 \int_{\xi=0}^{1-\eta} \left(\frac{e^{-jkR}-1}{R} \right) d\xi d\eta + \int_{\eta=0}^1 \int_{\xi=0}^{1-\eta} \frac{1}{R} d\xi d\eta, \quad (B4)$$

$$I_{\xi} = \int_{\eta=0}^1 \int_{\xi=0}^{1-\eta} \xi \left(\frac{e^{-jkR}-1}{R} \right) d\xi d\eta + \int_{\eta=0}^1 \int_{\xi=0}^{1-\eta} \xi \frac{1}{R} d\xi d\eta \quad (B5)$$

and

$$I_{\eta} = \int_{\eta=0}^1 \int_{\xi=0}^1 \eta \left(\frac{e^{-jkR}-1}{R} \right) d\xi d\eta + \int_{\eta=0}^1 \int_{\xi=0}^{1-\eta} \frac{\eta}{R} d\xi d\eta. \quad (B6)$$

The integrand of each of the first terms in (B5) - (B6) is non-singular and hence can be numerically integrated by using quadrature formulas for triangular regions obtained by Hammer et al. [21]. The remaining integrals in (B4) - (B6) are evaluated analytically by the following procedure.

We begin by expressing \bar{r}' in terms of area co-ordinates as

$$\bar{r}' = \bar{r}_1 + (\bar{r}_2 - \bar{r}_1) \xi + (\bar{r}_3 - \bar{r}_1) \eta, \quad (B7)$$

where \bar{r}_1 , \bar{r}_2 and \bar{r}_3 are the position vectors of the vertices of the source triangle. Hence,

$$\begin{aligned} R = |\bar{r} - \bar{r}'| &= |(\bar{r} - \bar{r}_1) - (\bar{r}_2 - \bar{r}_1) \xi - (\bar{r}_3 - \bar{r}_1) \eta| \\ &= [A\xi^2 + B\eta^2 + C\xi + D\eta + E\xi\eta + F]^{\frac{1}{2}}, \end{aligned} \quad (B8)$$

where

$$\begin{aligned} A &= |\bar{r}_2 - \bar{r}_1|^2, \\ B &= |\bar{r}_3 - \bar{r}_1|^2, \\ C &= -2(\bar{r} - \bar{r}_1) \cdot (\bar{r}_2 - \bar{r}_1), \\ D &= -2(\bar{r} - \bar{r}_1) \cdot (\bar{r}_3 - \bar{r}_1), \\ E &= 2(\bar{r}_2 - \bar{r}_1) \cdot (\bar{r}_3 - \bar{r}_1), \end{aligned} \quad (B9)$$

and

$$F = |\bar{r} - \bar{r}_1|^2.$$

With these definitions, the second integral in (B4) can be expressed as

$$I' = \int_{\eta=0}^1 \int_{\xi=0}^{1-\eta} \frac{d\xi d\eta}{[A\xi^2 + B\eta^2 + C\xi + D\eta + E\xi\eta + F]^{\frac{1}{2}}}. \quad (B10)$$

Next, making use of (2.261) of Gradshteyn and Ryzhik [26], one obtains from (B10)

$$I' = \frac{1}{|\bar{r}_2 - \bar{r}_1|} \left\{ \int_{\eta=0}^1 \ln \left[\sqrt{A_1 \eta^2 + B_1 \eta + C_1} + D_1 \eta + E_1 \right] d\eta \right. \\ \left. - \int_{\eta=0}^1 \ln \left[\sqrt{A_2 \eta^2 + B_2 \eta + C_2} + D_2 \eta + E_2 \right] d\eta \right\} \quad (B11)$$

where

$$A_1 = |\bar{r}_3 - \bar{r}_2|^2,$$

$$B_1 = -2(\bar{r}_3 - \bar{r}_2) \cdot (\bar{r} - \bar{r}_2),$$

$$C_1 = |\bar{r} - \bar{r}_2|^2,$$

$$D_1 = (\bar{r}_2 - \bar{r}_1) \cdot (\bar{r}_3 - \bar{r}_2) / |\bar{r}_2 - \bar{r}_1|,$$

$$E_1 = -(\bar{r}_2 - \bar{r}_1) \cdot (\bar{r} - \bar{r}_2) / |\bar{r}_2 - \bar{r}_1|,$$

$$A_2 = |\bar{r}_3 - \bar{r}_1|^2,$$

$$B_2 = -2(\bar{r}_3 - \bar{r}_1) \cdot (\bar{r} - \bar{r}_1),$$

$$C_2 = |\bar{r} - \bar{r}_1|^2,$$

$$D_2 = \frac{(\bar{r}_2 - \bar{r}_1) \cdot (\bar{r}_3 - \bar{r}_1)}{|\bar{r}_2 - \bar{r}_1|},$$

and

$$E_2 = - \frac{(\bar{r}_2 - \bar{r}_1) \cdot (\bar{r} - \bar{r}_1)}{|\bar{r}_2 - \bar{r}_1|}.$$

The remaining integrals in (B11) are both of the form

$$I_A = \int_{\eta=0}^1 \ln \left[\sqrt{A_1 \eta^2 + B_1 \eta + C_1 + D_1 \eta + E_1} \right] d\eta. \quad (B12)$$

With the substitution $x = D_1 \eta + E_1$, equation (B12) reduces to

$$I_A = \frac{1}{D_1} \int_{x=E_1}^{D_1+E_1} \ln \left[\sqrt{ax^2 + bx + c + x} \right] dx, \quad (B13)$$

where

$$a = A_1/D_1^2,$$

$$b = \frac{B_1 D_1 - 2A_1 E_1}{D_1^2}$$

$$c = \frac{C_1 D_1^2 - B_1 E_1 D_1 + A_1 E_1^2}{D_1^2}$$

and, in terms of the variable x , $R = \sqrt{ax^2 + bx + c}$. Eq. (B13) may be written as

$$D_1 I_A = I_1 = \int_{x=E_1}^{D_1+E_1} \ln (R+x) dx \quad (B14)$$

and hence the problem is reduced to evaluating the integral

$$I_1 = \int_{x_1}^{x_2} \ln (R+x) dx. \quad (B15)$$

By some elementary substitutions and integration by parts, I_1 may be written

as

$$I_1 = \left[x \ln(R+x) - R \right] \Big|_{x_1}^{x_2} + I_2 \quad (B16)$$

where

$$I_2 = \int_{x_1}^{x_2} \frac{(a-1)x + \frac{b}{2}}{(R+x)} dx.$$

Next, we note that

$$\begin{aligned} \frac{(a-1)x + \frac{b}{2}}{R+x} &= \frac{\left[x + \frac{b}{2(a-1)} \right] [R-x] [a-1]}{R^2 - x^2} \\ &= \frac{\left[x + \frac{b}{2(a-1)} \right] [R-x]}{\left[x + \frac{b}{2(a-1)} \right]^2 + \frac{c}{a-1} - \frac{b^2}{4(a-1)^2}}. \end{aligned}$$

Defining

$$u = x + \frac{b}{2(a-1)}$$

and

$$d^2 = \frac{c}{a-1} - \frac{b^2}{4(a-1)^2},$$

I_2 may be written as

$$I_2 = \int_{u=u_1}^{u_2} \frac{uR}{u^2 + d^2} du - \int_{u=u_1}^{u_2} \frac{u^2}{u^2 + d^2} du + \frac{b}{2(a-1)} \int_{u=u_1}^{u_2} \frac{u}{u^2 + d^2} du, \quad (B17)$$

where

$$u_1 = x_1 + \frac{b}{2(a-1)}$$

$$u_2 = x_2 + \frac{b}{2(a-1)}.$$

We note at this point that d^2 is always greater than or equal to zero, as can be easily verified by noting that $R^2 - x^2$ is greater than or equal to zero for all x . The last two integrals in (B17) may be integrated with the aid of tables and the result combined with (B16) to yield

$$I_1 = [x \ln (R + x) - R - x - d \tan^{-1} \frac{u}{d} + \frac{b}{4(a-1)} \ln \left(\frac{R^2 - x^2}{a-1} \right)] \Big|_{x_1}^{x_2} + I_3, \quad (B18)$$

where

$$I_3 = \int_{u_1}^{u_2} \frac{uR}{u^2 + d^2} du.$$

With the substitution $z = u + jd$, I_3 can be written as

$$I_3 = \operatorname{Re} \left[\int_{u_1}^{u_2} \frac{R}{z} dz \right].$$

Using Eq. 2.267.1 of [26] and taking the real part with some straight-forward but tedious algebra, one obtains

$$I_1 = \left\{ \left[x + \frac{b}{2(a-1)} \right] \ln (R+x) - x - \frac{b}{2\sqrt{a} (a-1)} \ln |2\sqrt{a} R + 2ax + b| + d \left[\tan^{-1} \frac{u}{d} - \tan^{-1} \frac{2dR(a-1)}{bx + 2c} \right] \right\} \Big|_{x=x_1}^{x_2} \quad (B19)$$

Combining the results of all these steps, one may now write I' as

$$\begin{aligned}
 I' = & \frac{1}{|\bar{r}_2 - \bar{r}_1|} \sum_{i=1}^2 \frac{(-1)^i}{D_i} \left\{ u_i \ln (R_i + x_i) \right. \\
 & - \frac{b_i}{2\sqrt{a_i} (a_i - 1)} \ln |2\sqrt{a_i} R_i + 2a_i x_i + b_i| \\
 & \left. + d_i \tan^{-1} \left(\frac{u_i}{d_i} \right) - d_i \tan^{-1} \left[\frac{2d_i R_i (a_i - 1)}{b_i x_i + 2c_i} \right] \right\} \Bigg|_{\eta=0}^1 \quad (B20)
 \end{aligned}$$

where

$$R_i = \sqrt{A_i \eta^2 + B_i \eta + C_i},$$

$$U_i = x_i + \frac{b_i}{2(a_i - 1)},$$

$$X_i = D_i \eta + E_i,$$

$$A_i = |\bar{r}_3 - \bar{r}_1|^2,$$

$$B_i = -2(\bar{r}_3 - \bar{r}_1) \cdot (\bar{r} - \bar{r}_1),$$

$$C_i = |\bar{r} - \bar{r}_1|^2,$$

$$D_i = \frac{(\bar{r}_2 - \bar{r}_1) \cdot (\bar{r}_3 - \bar{r}_1)}{|\bar{r}_2 - \bar{r}_1|},$$

$$E_i = - \frac{(\bar{r}_2 - \bar{r}_1) \cdot (\bar{r} - \bar{r}_1)}{|\bar{r}_2 - \bar{r}_1|},$$

$$a_i = A_i/D_i^2,$$

$$b_i = (B_i D_i - 2A_i E_i)/D_i^2,$$

$$c_i = (C_i D_i^2 - B_i D_i E_i + A_i E_i^2)/D_i^2,$$

$$d_i^2 = \frac{c_i}{a_i - 1} - \frac{b_i^2}{4(a_i - 1)^2}.$$

Some comments concerning the evaluation of (B20) are in order: 1) If either D_1 or D_2 is zero (which happens whenever the corner of the triangle at \bar{r}_1 , or r_2 , respectively, forms a right angle), Eq. (B20) cannot be evaluated in the form indicated. A simple way to circumvent this difficulty is to cyclically permute the assignment of vectors \bar{r}_1 , \bar{r}_2 and \bar{r}_3 to the corners of the triangle until neither D_1 nor D_2 is zero, i.e. until the right angle corner is placed at \bar{r}_3 . Under this new assignment of vertex indices, (B20) is valid. 2) The argument of either of the logarithmic terms appearing in (B20) may vanish for certain combinations of parameters. Whenever this situation occurs, however, the corresponding coefficient of the logarithmic term also vanishes and, by L'Hospital's rule, the product can be shown to vanish as well.

At this stage, all that remains is to evaluate the singular integrals in (B5) and (B6). Consider the pair of integrals,

$$I_P = \int_{\eta=0}^1 \int_{\xi=0}^{1-\eta} \frac{\xi d\xi d\eta}{R} \quad (\text{B21a})$$

and

$$I_Q = \int_{\eta=0}^1 \int_{\xi=0}^{1-\eta} \frac{\eta d\xi d\eta}{R}, \quad (B21b)$$

where

$$R = \left[A\xi^2 + B\eta^2 + C\xi + D\eta + E\xi\eta + F \right]^{\frac{1}{2}}.$$

With $a_1 = A$, $b_1 = C + E\eta$ and $C_1 = B\eta^2 + D\eta + F$, we have

$$R = \left[a_1 \xi^2 + b_1 \xi + C_1 \right]^{\frac{1}{2}}.$$

Using Eq. 380.011 of [27], one obtains for (B21a),

$$\begin{aligned} I_P = & \int_{\eta=0}^1 \frac{1}{A} \left[\eta^2 (A+B-E) + \eta (-2A-C+D+E) + A+C+F \right]^{\frac{1}{2}} d\eta \\ & - \frac{1}{A} \int_{\eta=0}^1 [B\eta^2 + D\eta + F]^{\frac{1}{2}} d\eta - \frac{C}{2A} \int_{\eta=0}^1 \int_{\xi=0}^{1-\eta} \frac{d\xi d\eta}{R} \\ & - \frac{E}{2A} \int_{\eta=0}^1 \int_{\xi=0}^{1-\eta} \frac{\eta d\xi d\eta}{R}. \end{aligned} \quad (B22)$$

One notes that the last two integrals in (B22) are I' , evaluated earlier, and I_Q of (B21b). Again using Eq. 380.201 of [27] and evaluating the first two integrals in (B22), one obtains

$$I_P = \frac{J_1 - J_2}{A} - \frac{C}{2A} I' - \frac{E}{2A} I_Q \quad (B23)$$

where

$$J_1 = \frac{(2B-C+D+E)(\sqrt{B+D+F}) + (2A+C-D-E)(\sqrt{A+C+F})}{4(A+B-E)} \\ + \frac{4(A+C)(B+D+F) + 4F(B-C-E) - (C+D+E)^2}{8(A+B-E)^{3/2}} \\ \times \ln \left| \frac{2\sqrt{(A+B-E)(B+D+F)} + (2B-C+D-E)}{2\sqrt{(A+B-E)(A+C+F)} - (2A+C-D-E)} \right|$$

and

$$J_2 = \frac{(2B+D)(\sqrt{B+D+F}) - D\sqrt{F}}{4B} \\ + \frac{4BF-D^2}{8B\sqrt{B}} \ln \left| \frac{2\sqrt{B(B+D+F)} + 2B+D}{2\sqrt{BF} + D} \right|.$$

Adopting the same procedure, I_Q in (B21b) can be written as

$$I_Q = \frac{J_3 - J_4}{B} - \frac{D}{2B} I' - \frac{E}{2B} I_P, \quad (B24)$$

where

$$J_3 = \frac{(2A+C-D-E)(\sqrt{A+C+F}) + (2B-C+D-E)(\sqrt{B+D+F})}{4(A+B-E)} \\ + \frac{4(A+C)(B+D+F) + 4F(B-C-E) - (C+D+E)^2}{8(A+B-E)^{3/2}} \\ \times \ln \left| \frac{2\sqrt{(A+B-E)(A+C+F)} + (2A+C-D-E)}{2\sqrt{(A+B-E)(B+D+F)} - (2B-C+D-E)} \right|$$

and

$$J_4 = \frac{(2A+C)(\sqrt{A+C+F}) - C\sqrt{F}}{4A} \\ + \frac{4AF-C^2}{8A\sqrt{A}} \ln \left| \frac{2\sqrt{A(A+C+F)} + 2A+C}{2\sqrt{AF} + C} \right|.$$

Equations (B23) and (B24) may be solved simultaneously for the unknown integrals I_P and I_Q to obtain

$$I_P = \frac{4B(J_1 - J_2) - 2E(J_3 - J_4) - (2BC - ED) I'}{4AB - E^2} \quad (B25)$$

and

$$I_Q = \frac{4A(J_3 - J_4) - 2E(J_1 - J_2) - (2AD - EC) I'}{(4AB - E^2)} \quad (B26)$$

This completes the analytical evaluation of the singular integrals.

REFERENCES

- [1] J.H. Wang, "A wire-grid model for scattering by conducting bodies," IEEE Trans. Antennas Propagat., Vol. AP-14, No. 6, pp. 782-786, Nov. 1966.
- [2] E.K. Miller and F. J. Deadrick, "Some computational aspects of thin-wire modeling," in Numerical and Asymptotic Techniques in Electromagnetics, R. Mittra, Ed., New York: Springer-Verlag, 1975, Chapt. 4.
- [3] K.S.H. Lee, L. Marin, and J.P. Castillo, "Limitations of wire-grid modeling of a closed surface," IEEE Trans. Electromagn. Compat., Vol. EMC-18, No. 3, pp. 123-129, Aug. 1976.
- [4] D.L. Knepp and J. Goldhirsh, "Numerical analysis of electromagnetic radiation properties of smooth conducting bodies of arbitrary shape," IEEE Trans. Antennas Propagat., Vol. AP-20, No. 3, pp. 383-388, May 1972.
- [5] N.C. Albertsen, J.E. Hansen, and N.E. Jenson, "Computation of radiation from wire antennas on conducting bodies," IEEE Trans. Antennas Propagat., Vol. AP-22, No. 2, pp. 200-206, March 1974.
- [6] G.J. Burke and A.J. Poggio, "Numerical Electromagnetic Code (NEC) - method of moments," Technical Document 116, AFWL-TR-76-320, Naval Ocean Systems Center, San Diego, CA, July 1977.
- [7] N.N. Wang, J.H. Richmond, and M.C. Gilreath, "Sinusoidal reaction formulation for radiation and scattering from conducting surfaces," IEEE Trans. Antennas Propagat. Vol. AP-23, No. 3, pp. 376-382, May 1975.
- [8] A. Sankar and T.C. Tong, "Current computation on complex structures by finite element method," Electronics Letters, Vol. 11, No. 20, pp. 481-482, Oct. 1975.
- [9] J.J.H. Wang, "Numerical analysis of three-dimensional arbitrarily-shaped conducting scatterers by trilateral surface cell modelling," Radio Science, Vol. 13, No. 6, pp. 947-952, Nov.-Dec. 1978.
- [10] J.J.H. Wang and C. Papanicolopoulos, "Surface patch modeling of scatterers of arbitrary shapes," AP-S Int. Symp. Digest, University of Washington, Seattle, June 1979, pp. 159-162.
- [11] G. Jeng and A. Wexler, "Finite element, boundary integral equation analysis of scattering problems," URSI Symp. on Electromagnetic Wave Theory, Stanford University, Stanford, June 1977, pp. 179-181.
- [12] J. Singh and A.T. Adams, "A non-rectangular patch model for scattering from surfaces," IEEE Trans. Antennas Propagat., Vol. AP-27, No. 4, pp. 531-535, July 1979.
- [13] R.F. Harrington, Field Computation by Moment Methods. New York: Macmillan, 1968.

- [14] S.S.M. Rao, A.W. Glisson, D.R. Wilton, and B.S. Vidula, "A simple numerical solution procedure for statics problems involving arbitrarily-shaped surfaces," to appear in IEEE Trans. Antennas Propagat., Sept 1979.
- [15] A.W. Glisson and D.R. Wilton, "Simple and efficient numerical methods for problems of electromagnetic radiation and scattering from surfaces," submitted to IEEE Trans. Antennas Propagat. Also see notes from Numerical and Asymptotic Techniques for Electromagnetics and Antennas short course sponsored by Syracuse University and the University of Illinois, Blue Mountain Lake, NY, Sept. 1979.
- [16] J.R. Mautz and R.F. Harrington, "Electromagnetic scattering from a homogeneous material body of revolution," AEÜ, Vol. 33, No. 2, pp. 71-80, Feb. 1979.
- [17] J.R. Mautz and R.F. Harrington, "H-Field, E-Field, and combined-field solutions for conducting bodies of revolution," AEÜ, Vol. 32, No. 4, pp. 157-164, April 1978.
- [18] A.W. Glisson, "On the development of numerical techniques for treating arbitrarily-shaped surfaces," Ph.D. dissertation, Univ. of Mississippi, 1978.
- [19] J. Van Bladel, Electromagnetic Fields. New York: McGraw-Hill, 1964.
- [20] O.C. Zienkiewicz, The Finite Element Method in Engineering Science. New York: McGraw-Hill, 1971.
- [21] P.C. Hammer, O.P. Marlowe, and A.H. Stroud, "Numerical integration over simplexes and cones," Math. Tables Aids Comp., 10, pp. 130-137, 1956.
- [22] A.J. Poggio and E.K. Miller, "Integral equation solutions of three-dimensional scattering problems," in Computer Techniques for Electromagnetics, R. Mittra, Ed., New York: Pergamon, 1973.
- [23] J.J. Bowman, T.B.A. Senior, and P.L.E. Uslenghi, Electromagnetic and Acoustic Scattering by Simple Shapes. Amsterdam: North-Holland, 1969, pp. 576-577.
- [24] O.C. Zienkiewicz and D.V. Phillips, "An automatic mesh generation scheme for plane and curved surfaces by 'isoparametric' co-ordinates," International Journal for Numerical Methods in Engr., Vol. 3, pp. 519-528, 1971.
- [25] B. O'Neill, Elementary Differential Geometry. New York: Academic Press, 1966.
- [26] I.S. Gradshteyn and I.M. Ryzhik, Tables of Integrals, Series and Products. New York: Academic Press, 1965.
- [27] H.B. Dwight, Tables of Integrals and Other Mathematical Data. New York: Macmillan, 1961.

A decorative rectangular border with a repeating scroll-like pattern surrounds the central text.

MISSION of Rome Air Development Center

RADC plans and executes research, development, test and selected acquisition programs in support of Command, Control Communications and Intelligence (C³I) activities. Technical and engineering support within areas of technical competence is provided to ESD Program Offices (POs) and other ESD elements. The principal technical mission areas are communications, electromagnetic guidance and control, surveillance of ground and aerospace objects, intelligence data collection and handling, information system technology, ionospheric propagation, solid state sciences, microwave physics and electronic reliability, maintainability and compatibility.